Cooling and Trapping a Bose-Fermi Mixture of Dilute Atomic Gases

Refroidissement et Piégeage d'un Mélange Bose-Fermi de Gaz Atomiques Dilués

Martin Zwierlein

Stage de Recherche, MIP 2e Année

Massachusetts Institute of Technology

Research Laboratory of Electronics, MIT-Harvard Center for Ultracold Atoms and Department of Physics

Thesis Advisor: Wolfgang Ketterle
Title: John D. MacArthur Professor of Physics

Research Laboratory for Electronics, MIT-Harvard Center for Ultracold Atoms, and Department of Physics
Massachusetts Institute of Technology, Room 26-243
77 Massachusetts Ave., Cambridge, MA 02139, USA
Tel. 1-617-253-6815, FAX 1-617-253-4876
E-mail: ketterle@mit.edu

Cambridge January 2001 - July 2001

To Erika and Otto,

Anju and Cornel

Contents

Chapter 1

Introduction

1.1 General Context

The achievement of Bose-Einstein-Condensation (BEC) in trapped, dilute, weakly interacting atomic gases [1] opened a whole new steadily growing field of atomic physics. Over the past six years, what started as the quest for the demonstration of BEC itself, has given rise to a much broader research both in conventional atomic physics and in what has traditionally been the area of condensed matter physics.
The natural extension of this work is the search for quantum degeneracy in Fermi gases. After the first experimental report on cooling a dilute Fermi gas to temperatures where quantum statistics are already pronounced, by DeMarco and Jin [2], this field has attracted large interest in both experimental and theoretical research.
What makes dilute Fermi gases, like their bosonic counterparts, particularly appealing is that they present an only weakly interacting system, where the effects of quantum statistics are not blurred by strong interactions. In addition, the strength of the particle interactions can be manipulated experimentally [3], giving a large control over the behaviour of the atoms.

The basic criterion for the onset of quantum degeneracy is independent of the particle statistics and simply requires that the thermal de Broglie wavelength λ_{dB} becomes comparable to the interatomic spacing, so that the particle wave functions overlap in real space: $n\lambda_{dB}^3 \sim 1$, where n is the particle density. For the same (harmonic) trapping potential as used in BEC experiments, and hence the same number of one-particle states, n will be on the same order of magnitude for Bose as for Fermi systems. Thus we find a Fermi temperature which is, up to a numerical prefactor ~ 1, the same as the condensation temperature in a Bose system, $T_F \sim \frac{\hbar\omega}{k_B} N^{1/3}$, where N is the total particle number and ω is the geometric mean of the trapping frequencies in three dimensions. For a typical cloud with trapping frequencies on the order of 100 Hz, and $N \sim 10^6$, this corresponds to the μK scale. It is below this characteristic temperature that the Fermi and Bose gases start differing drastically. While bosons undergo a phase transition and start piling up in the ground state of the system, fermions are forced to occupy orthogonal states.

For most part, the experimental techniques of laser cooling and magnetic trapping, as well as imaging the Fermi gas, are essentially the same as those used in BEC experiments [4]. However, the final and crucial cooling stage towards BEC, evaporative cooling, relies on rethermalization of the gas through elastic s-wave collisions. In a spin-polarized Fermi gas, particles cannot be in a symmetric spatial state, and the dominant interaction must be p-wave scattering. This scattering channel is strongly inhibited by the presence of the centrifugal barrier, already at temperatures below $\sim 100\,\mu$K [5, 6]. The solution to this problem is to load two different species into the magnetic trap, allowing efficient rethermalization through inter-species collisions. In [2, 7], this sympathetic cooling has been achieved with different spin-states of potassium-40, reaching temperatures of $T/T_F = 0.25$. Double species experiments with two Li-isotopes have led to temperatures of $T/T_F = 0.2$ [8, 9] and demonstrated Pauli blocking of the fermionic isotope ^{6}Li. Therefore, sympathetic cooling gives the perspective to study condensed matter properties of Fermi systems at ultra-low temperatures in the quantum degenerate regime.

A challenging goal in the study of degenerate Fermi gases is the observation of a BCS-like phase transition (Bardeen, Cooper, Schrieffer). When in a bosonic system like ^{4}He a macroscopic number of particles occupies the ground state, the atoms delocalize and the system becomes superfluid. In dilute atomic gases, superfluidity of a BEC has been demonstrated [10] and the formation of vortex lattices has been observed [11, 12], in analogy to the "rotating bucket" experiments with ^{4}He. For fermionic systems, like ^{3}He, a superfluid phase seems not possible, since every particle must occupy different states. However, metals at low temperature become superconducting: The fermionic electrons form so-called Cooper pairs, bosons, which can condense. Likewise, ^{3}He can become superfluid by Cooper-pairing of two ^{3}He-atoms.
The transition temperature for that effect scales as

$$T_C \sim \frac{\epsilon_F}{k_B} \exp -\frac{\pi}{2k_F|a|}, \tag{1.1}$$

where $\epsilon_F = (\hbar k_F)^2/2m$ and k_F are the Fermi energy and momentum and $|a|$ is the value of the negative scattering length. For ^{6}Li, Hulet et. al. [13] have measured a large, attractive triplet scattering length, $a_T = -2160 \pm 250\,\mathrm{a_0}$ (Bohr radius a_0 $0.5A$). For a Fermi temperature of $T_F \sim 1\,\mu$K this gives a transition temperature of $T_C \sim 0.05T_F$. For higher temperatures it may be possible to tune the scattering length by magnetic fields. In the vicinity of Feshbach resonaces one can achieve extremely large scattering lengths [3]. Therefore, one might be able to increase the transition temperature to values accessible by experiment and to observe Cooper-pairing of atoms in a dilute Fermi gas.

1.2 This Thesis

In this thesis we describe a new double species experiment with ^{23}Na and ^{6}Li in Wolfgang Ketterle's group at MIT. The use of sodium and lithium promises to achieve lower temperatures than for instance in ^{6}Li-^{7}Li experiments by exploiting the difference in mass of both species as well as the high atom number and the stability of the sodium condensate [1].

To achieve the goal of cooling and trapping two species of atoms, an existing sodium BEC machine has been equipped with a double-species oven. A diode laser system for ^{6}Lihas been built which generates the slowing, trapping and imaging light for the atoms. In a test stage experiment, a lithium-only MOT was created in a separate laboratory. Then the laser system was moved to the BEC machine and the laser light for sodium and lithium was merged. This resulted in a double-species MOT of 10^{10} sodium atoms and up to 10^{8} lithium atoms.

The thesis begins in chapter two with a review on cooling and trapping techniques in dilute atomic gases, common to BEC and Degenerate Fermi Gas experiments. We present the principle of laser cooling and magneto-optical trapping and point out the frequency needs for a lithium laser system. The description of this system, the central part of this thesis, is given in chapter three. We will focus on the laser frequency stabilization scheme and the creation of the imaging light used to image the atoms in the trap. Finally, chapter four presents the double-species MOT achieved with sodium and lithium. We perform measurements on the atom number and determine the temperature of the atoms in the ^{6}Li-MOT. A first experiment on cold collisions between sodium and lithium in the double-species MOT is included. We close with an outlook on further steps towards quantum degeneracy.

[1] Although recently the ^{6}Li-^{7}Li experiment in Paris led to the achievement of a stable ^{7}Li condensate [9]

Chapter 2

Experimental Techniques of Slowing, Trapping and Cooling Atoms

2.1 Atomic Properties of Alkalis

The underlying idea of the field of laser cooling and trapping is to use our knowledge about the internal structure of atoms to manipulate their external degrees of freedom. It is therefore worthwhile to summarize some basic atomic properties.

Relevant Electronic States

The ground state of an alkali atom has an "unpaired" electron in the S shell, $2^2S_{1/2}$ for lithium and $3^2S_{1/2}$ for sodium. The first excited state is of the form n^2P_J and is split by spin-orbit ($\vec{L}\cdot\vec{S}$) coupling into $J = 1/2$ and $J = 3/2$ states. We will be concerned only with the $n^2P_{3/2}$ state, connected to the ground state by the 'D_2'-line. The wavelength corresponding to this transition is 671 nm for lithium and 589 nm for sodium. The fact that this lies in the visible and is readily accessible with laser light is part of the reason why alkali atoms are attractive for laser cooling and trapping.

Both the ground and the excited state are further split by the coupling between the electron and the nuclear spin I, $\propto \vec{I}\cdot\vec{J}$. At low magnetic fields, the good quantum numbers are therefore $\vec{F} = \vec{I}+\vec{J}$, and its projection along the quantization axis, m_F. The value of the nuclear spin is $I = 1$ in ^{6}Li and $I = 3/2$ in ^{23}Na. The hyperfine splitting of the ground state is 228 MHz in ^{6}Li and 1.77 GHz in ^{23}Na.

Of particular interest for laser cooling are the so-called "fully stretched" states, for which all the angular momenta of the electron and the nucleus are lined up on the quantization axis: $|m_F| = F = I+J = I+L+S$. The ground and the excited stretched state, with the same sign of m_F, form a closed "cycling" transition. By this we mean that if an atom is optically excited from the former to the latter, with a circularly polarized light, selection rules prevent it from falling back anywhere else but where it started from. This subset of states thus represents an almost ideal two level system.

In fig. 2-1, 2-2, the relevant energy levels for sodium and lithium are depicted. For both species, the cycling transition is shown, as well as the so-called repumping transition. The

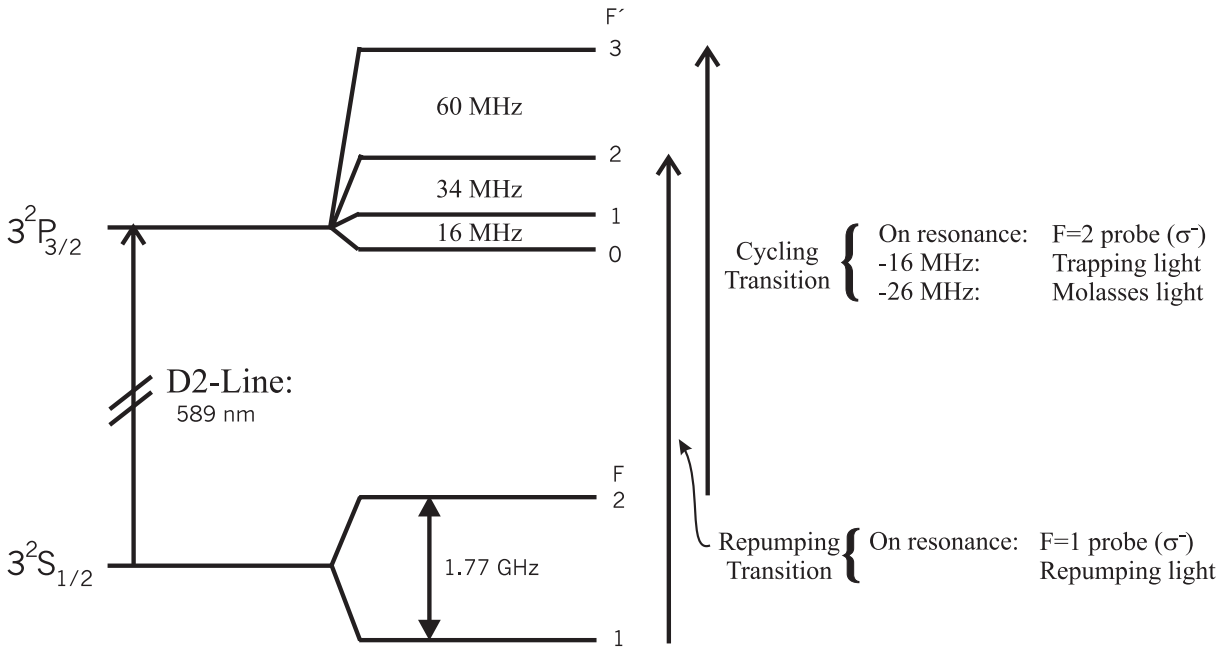

Figure 2-1: *Level Diagram for ^{23}Na showing hyperfine structure for the $3^2S_{1/2}$ ground state and the $3^2P_{3/2}$ excited state. Light used for $F = 2$ probing, trapping, and polarization-gradient cooling is on- or near-resonance with the $|F = 2\rangle \rightarrow |F' = 3\rangle$ cycling transition. $F = 1$ probing and repumping light is resonant with the $|F = 1\rangle \rightarrow |F' = 2\rangle$ transition, and thus 1.77 GHz blue-detuned from the cycling transition. Slowing light is 1 GHz red-detuned from the cycling transition.*

need for the latter arises from the finite probability of exciting the wrong upper hyperfine levels. From there, the electron may fall into the "dark" ground state and would be lost for further cycles. Light at the repumping frequency has to excite those "lost" atoms back to the upper hyperfine levels from which they eventually fall back into the "right" ground state. For sodium, only a small amount of light (5% of the total) is needed at the repumping transition. However, in ^{6}Li, the upper hyperfine states are not resolved (level-spacing less than the natural linewidth Γ). Therefore, chances are high that one excites the wrong level. The light intensity at the repumping transition therefore has to be as strong as that at the cycling transition.

Magnetic Properties

If we ignore the small nuclear contribution, all of the atom's magnetic moment comes from the one unpaired electron. This moment is of the order of one Bohr magneton, $\mu_B = \hbar \times 1.4\,\mathrm{MHz/G}$. This in fact is the second reason that makes alkali atoms suitable for laser cooling and trapping. As we shall describe below, tunability of atomic energy levels by magnetic fields is at the heart of Zeeman slowing, magneto-optical trapping, and magnetic trapping.

In terms of good (low magnetic field) quantum numbers, the atom's magnetic moment takes the form $\mu = -g_F m_F \mu_B$. To find the value of the Landé g_F-factor, we project the

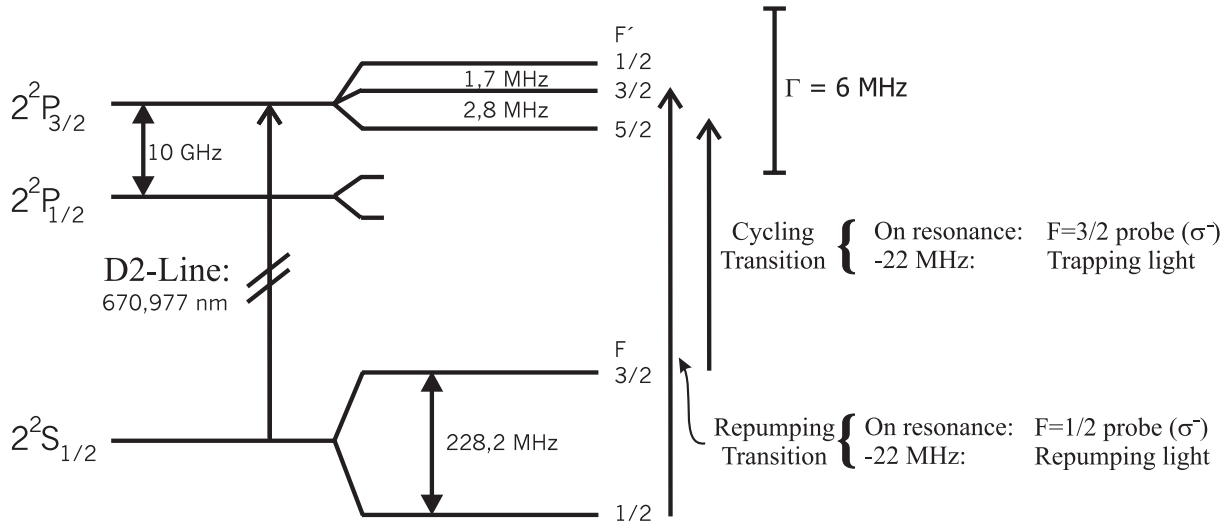

Figure 2-2: *Level Diagram for ^6Li showing hyperfine structure for the $2^2S_{1/2}$ ground state and the $2^2P_{3/2}$ excited state. Here, the upper hyperfine levels are not resolved. Light used for $F = 3/2$ probing and trapping is on- or near-resonance with the $|F = 3/2\rangle \rightarrow |F' = 5/2\rangle$ cycling transition, but $|F' = 1/2\rangle$ and $|F' = 3/2\rangle$ are also affected. $F = 1/2$ probing and repumping light is resonant with the $|F = 1/2\rangle \rightarrow |F' = 1/2, 3/2\rangle$ transition, 228 MHz blue-detuned from the cycling transition.*

electron orbital and spin contributions to the magnetic moment onto the total atomic spin ($\vec{F}$). In the ground state of all alkali atoms, the g_F factor universally takes a simple form $g_{F=I\pm1/2} = \pm 1/(I + 1/2)$. At higher magnetic fields, the separate magnetic energies of the nuclear and the electron spins must be accounted for, as described by the Breit-Rabi formula [14]. This gives rise to a low-field quadratic Zeeman shift and the eventual decoupling of the electron and nuclear spin at high field. Fig. 2-3 shows the energies of hyperfine states of sodium and lithium in a magnetic field. The implications for magnetic trapping are described in section 2.5.

2.2 Laser Cooling

As described before, when exciting a cycling transition, the atom behaves like a two-level system. Let us denote $E_e - E_g = \hbar\omega_0$ the level-separation in energy, the dipole matrix element connecting the two levels $D = -e\langle e\,|r|\,g\rangle$, and the corresponding excited state decay rate (or natural linewidth) Γ. Coupling of the two states by an electric field of the form $E = E_0\cos(\omega t)$ is conveniently expressed in terms of the Rabi frequency $\Omega_R \equiv (1/\hbar)E_0 D$. We can then express the intensity of a laser beam in a dimensionless form, in terms of the saturation parameter $s_0 \equiv 2\Omega_R^2/\Gamma^2$. In equilibrium, the rate at which the system absorbs photons from the laser beam must be equal to the rate at which it spontaneously emits them. This rate is equal to the product of the excited state's occupation and decay rate Γ, and we can calculate it to be:

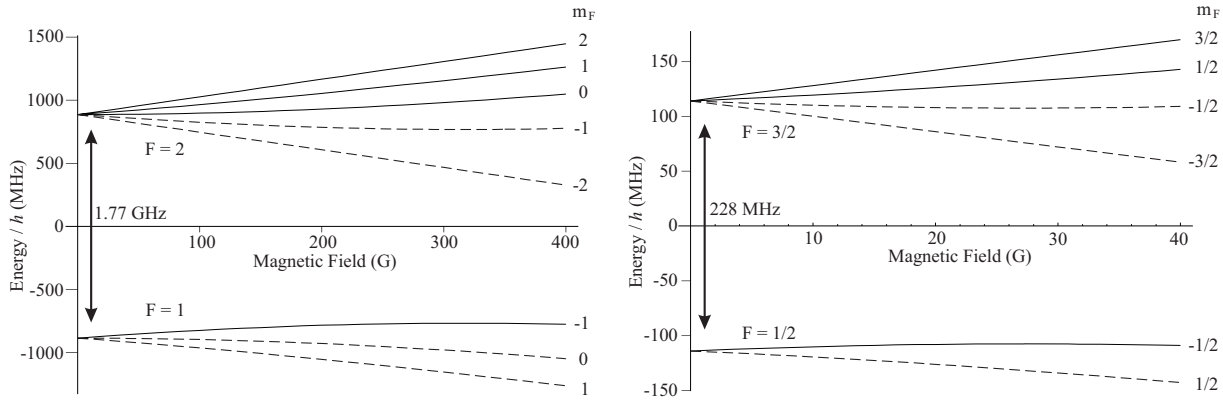

Figure 2-3: *Energies of hyperfine states of sodium and lithium in a magnetic field. States with a total spin $F = 2$ and $F = 3/2$ at zero field are shown in the top of the respective figures, those with $F = 1$ and $F = 1/2$ at the bottom. The quantum number m_F of the spin-projection on the magnetic field axis is shown at right. Solid lines indicate weak-field seeking, magnetically-trappable states at low field. States indicated with dashed lines cannot be magnetically trapped.*

$$\Gamma_s = \frac{\Gamma}{2} \frac{s_0}{1 + s_0 + (2\delta/\Gamma)^2} \tag{2.1}$$

where the detuning $\delta = \omega - \omega_0$.

Natural linewidths in lithium and sodium are $2\pi \times 6\,\mathrm{MHz}$ and $2\pi \times 10\,\mathrm{MHz}$ respectively. So an atom can scatter a photon about every 40 ns. Saturation intensity, corresponding to $s_0 = 1$ defines the separation between 'high' and 'low' intensities. Its value is approximately $2.5\,\mathrm{mW/cm^2}$ in lithium, and $6.4\,\mathrm{mW/cm^2}$ in sodium.

Spontaneous Light Force

Every time an atom absorbs a photon, it receives a momentum kick of $\Delta\vec{p} = \hbar k$ where k is the photon wave vector. If it subsequently emits another photon by spontaneous emission, this will occur in a regular dipole pattern, which means that probabilities of emission are equal for opposite directions. Therefore, the average over many spontaneous emissions results in no net momentum change. One absorption-emission cycle lasts $\Delta t = 1/\Gamma_s$. Consequently, there will be a net force on the atom, called spontaneous light force, expressed by

$$\vec{F} = \frac{\Delta\vec{p}}{\Delta t} = \hbar\vec{k}\Gamma_s. \tag{2.2}$$

Atoms moving with a velocity $\vec{v}$ in the direction of the laser light experience the Doppler shift $-\vec{k} \cdot \vec{v}$. This is to be included in Eq. 2.1 by changing $\delta \to \delta - \vec{k} \cdot \vec{v}$. We thereby see that an atom moving in isotropic red detuned light experiences the momentum kick preferentially in the direction opposite to its motion. This effect is at the basis of laser slowing and cooling.

Optical Molasses

Let us now consider two counterpropagating beams, with wave vector $\pm\vec{k}$ and detuned to the red of the atomic resonance by δ. They exert a net force on the atom which can be found by adding the respective expressions for the scattering force 2.2:

$$\vec{F}_{\rightarrow\leftarrow} = \frac{\hbar\vec{k}\Gamma}{2}\left(\frac{s_0}{1+s_0+(\frac{2(\delta-kv)}{\Gamma})^2} - \frac{s_0}{1+s_0+(\frac{2(\delta+kv)}{\Gamma})^2}\right). \tag{2.3}$$

If we assume that the atom's velocity is smaller than $v_c = \Gamma/k$ ($\approx$ 4m/s for lithium, $\approx$ 6m/s for sodium), we can expand the expression and get:

$$\approx \frac{8\hbar k^2 s_0 \delta}{\Gamma(1+s_0+(\frac{2\delta}{\Gamma})^2)^2}\cdot\vec{v} \equiv -\beta\vec{v}. \tag{2.4}$$

We thus find a damping force with damping constant β, which is sketched in fig. 2-4. The extension to three dimensions is straight-forward: Three pairs of counterpropagating laser beams create a viscous medium for the atoms, called optical molasses, in which they are slowed and cooled. This was first observed by Chu et al. [15] in a gas of sodium atoms.

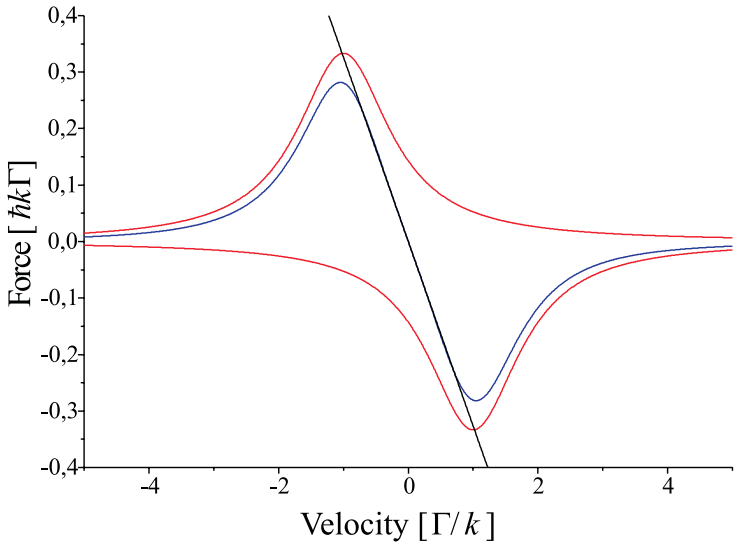

Figure 2-4: *Damping Force in one-dimensional optical molasses. Two counter-propagating laser beams with wave-vector $\vec{k}$ and detuning $-\delta$ to atomic resonance create a damping force for atoms slower than Γ/k. Shown are the contributions of each laser beam (in red) and their sum (in blue). The black line indicates the slope of the resulting force around zero velocity.*

Limits of Doppler-Cooling

The cooling process in optical molasses is opposed by heating due to the random nature of spontaneous emission. Stochastic spontaneous-photon recoils lead to diffusion in ve-

locity space and therefore to heating. When heating balances cooling, the cloud of atoms reaches a limiting temperature, called Doppler cooling temperature T_D. It depends on the intensity and the detuning of the cooling light and reaches a minimum

$$k_B T_D = \frac{\hbar\Gamma}{2},$$

achieved for low intensity and a detuning of $\delta = -\frac{\Gamma}{2}$ [16]. For sodium, this temperature is $T_D^{\mathrm{Na}} = 240\,\mu\mathrm{K}$, for lithium it is $T_D^{\mathrm{Li}} = 144\,\mu\mathrm{K}$.
Nevertheless, much lower temperatures are possible with laser-cooling, as observed by Lett et al. [17] and explained by Dalibard, Cohen-Tannoudji [18] and Ungar et al. [19]. The quite subtle cooling mechanism at work is called Sisyphus cooling or polarization-gradient cooling. It arises from the perpendicular polarizations of the counterpropagating laser beams and induced spatially varying light shifts of the atomic energy levels. When the atoms move in the resulting periodic potential of hills and valleys, they climb the hills more often than to descend to the valleys, leading to efficient cooling.

2.3 Magneto-Optical Trap

In optical molasses, the atoms are cooled but not confined in space, still being able to slowly drift away. The solution to that problem was proposed by J. Dalibard [20], and is summarized in figure 2-5. Consider a hypothetical atom with a S_0 ground state and a P_1 excited state placed in an inhomogeneous magnetic field $B(z) = bz$. If the atom is at zero magnetic field its Zeeman sublevels are degenerate, but as the atom moves along the z axis the levels split increasingly. At $z > 0$, it is the $m = -1$ sublevel whose energy is shifted down, whereas at $z < 0$, it is the $m = 1$-level. We now irradiate the atom with two counterpropagating laser beams of opposite helicity, σ_- for the beam propagating to the left, and σ_+ for the one propagating to the right. They excite transitions to the $m = -1$ and $m = +1$ levels respectively. If both beams are equally tuned to the red of the atomic resonance, then an atom at $z = 0$ will scatter on average an equal amount of photons from the left- as from the right-propagating beam. But, if the atom moves along the z-axis, the Zeeman effect shifts the m-levels, so that for instance at $z > 0$ the σ_--beam coming from the right is closer to resonance. Consequently, the resulting radiation force is always directed towards the origin and the atom is trapped.

The first MOT was realized in 1987 by Raab et. al. [21] in a sample of sodium atoms, and has since been the starting point of numerous experiments with cold atoms.

2.4 Zeeman Slowing of an Atomic Beam

The velocity an atom may have to be still captured in a MOT is comparable to that in Optical Molasses, which is a few times Γ/k, on the order of 10 m/s for ^{6}Li and ^{23}Na. To efficiently load the MOT, one therefore has to produce slow atoms.

The first method to have succeeded in slowing an atomic beam is Zeeman Slowing [22]. The atoms, coming out of an oven and being several 100° K hot, are irradiated by circularly

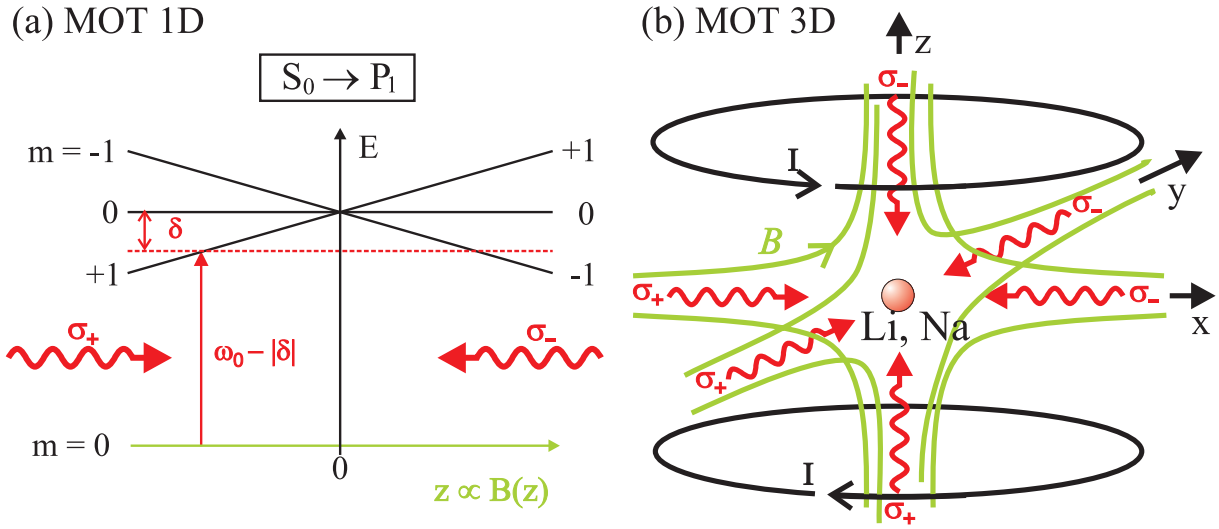

Figure 2-5: *The Magneto-Optical Trap. a) Situation in 1D. Due to the Zeeman shift in a linear magnetic field, the atoms at $z > 0$ ($z < 0$) scatter more photons from the right (left) laser beam with polarization σ_- (σ_+) and are thus repelled towards the center of the trap. b) 3D trapping scheme. Two coils carrying current I create a spherical quadrupole field, indicated by the green B-field lines.*

polarized laser light, red detuned from the atomic resonance and opposing their motion. Due to the Doppler effect, the atoms will eventually shift into resonance with the laser beam and decelerate according to

$$a = -\frac{\hbar k}{m}\Gamma_s,$$

which saturates at large s_0 to $a_{\max} = -\frac{\hbar k}{m}\frac{\Gamma}{2}$. However, after only a few cycles of absorption-emission of photons, the atoms would become too slow to absorb the light without further doing. By applying a well-tailored, spatially variable magnetic field along the moving atom's path, they may stay in resonance due to the Zeeman effect. For uniform deceleration from initial velocity v_0, the appropriate field profile is [23]

$$B(z) = B_0 + \Delta B\sqrt{1 - z/z_0}, \tag{2.5}$$

where B_0 is an optional offset magnetic field, $z_0 \equiv \frac{Mv_0^2}{\hbar k\gamma}$ is the length of the magnet and $\Delta B = \frac{\hbar k v_0}{\mu_B}$. We observe here that the optimal length of the magnet depends on the atom we want to decelerate. For the case of our double-species experiment, the Zeeman slower is optimized for sodium, but the lithium flux is still on the order of 10^7 slowed atoms per second arriving in the main chamber.

We use an increasing field Zeeman slower ($B_0 \simeq -\Delta B$ in 2.5). Atoms entering the slower from the oven are exposed to a small magnetic field and to slowing light with a $\Delta \simeq 1$ GHz detuning, corresponding to a capture velocity of $\Delta \cdot \lambda_{\mathrm{Na,Li}} \simeq 590$ m/s for Na and 670 m/s for Li. The field increases along the slower to about 700 G and is then quickly brought to zero at its end. The slowed atomic beam passes into the capture region of the MOT. Due to the large detuning, the slowing light may pass directly through the MOT

without affecting the loading.

2.5 Magnetic Trapping and Evaporative Cooling

For further cooling of the trapped sample of atoms, the constant resonant light scattering in a MOT is a handicap. Magnetic trapping provides a "cleaner" way of confining the atoms. In the presence of a magnetic field, the energy of an atom is shifted by an amount $U = -\vec{\mu} \cdot \vec{B}(\vec{r})$ where $\vec{B}(\vec{r})$ is the magnetic field at point $\vec{r}$, and $\vec{\mu}$ the magnetic moment of the atom as explained in section 2.1.

A magnetic trap creates a magnetic field which has a minimum of the field strength. This represents a trapping potential for atoms with a magnetic moment anti-aligned with the magnetic field, i.e. for low-field magnetic quantum states with $g_F m_F > 0$ (weak-field seekers) [1]. We use a Ioffe-Pritchard trap [25, 26], which solves the problem of "Majorana flops" (spin-flips to untrapped spin states) in regions for vanishing B-field.

Fig. 2-3 shows the energy levels of the electronic ground states of sodium and lithium in a magnetic field. The sodium atoms are trapped and cooled to the BEC transition in the $|F = 1, m_F = -1\rangle$ state. This leaves for lithium only the $|F = 1/2, m_F = -1/2\rangle$ state to be used for sympathetic cooling with sodium. The other trappable states, $|F = 3/2, m_F = 3/2\rangle$ and $|F = 3/2, m_F = 1/2\rangle$, would be expelled from the trap by spin-exchange collisions with sodium. Unfortunately, the $|F = 1/2, m_F = -1/2\rangle$ state becomes an untrapped state for magnetic fields stronger than 27 G. The trap-depth in temperature for that state is $T_{27\mathrm{G}} \approx 300\,\mu\mathrm{K}$. The temperatures attained in a MOT are usually larger than that. We will address this problem briefly in chapter 5.

The final and crucial step towards BEC in sodium is evaporative cooling, which was first demonstrated in atomic hydrogen [27] (a review on evaporative cooling is given in [31]). An RF-"knife" selectively flips the spin of "hot" atoms with kinetic energy higher than a certain truncation energy ϵ_t and thus kicks them out of the trap. The remaining atoms rethermalize by elastic collisions and therefore cool. Lowering ϵ_t results in a lower finite temperature but also in a lower number of surviving atoms.

Evaporative Cooling of spin-polarized ^{6}Li alone is not possible, since s-wave scattering between two Fermions with the same spin is prohibited, and p-wave scattering is highly suppressed for temperatures lower than $\sim 100\,\mu\mathrm{K}$ [5, 6]. The spatial part of the combined wave function of both particles has to be asymmetric. Therefore the probability to find them at the same point is zero. However, efficient cooling of ^{6}Li should be possible by elastic collisions with sodium ("sympathetic cooling") while the latter is being evaporated.

[1] high-field seekers ($g_F m_F < 0$) cannot be trapped since it is impossible to create a local maximum of a static magnetic field [24]

Chapter 3

Laser System for ^{6}Li

In this chapter we present the laser system which generates the slowing, trapping and imaging light for ^{6}Li. For the needed power of several tens of mW at a wavelength of 670nm, the obvious choice are laser diodes which are cheap and easy to handle. We describe the locking scheme used to stabilize the lasers to an atomic resonance, which is reliable and accurate to less than a MHz. To monitor the absorption of a probe beam by the cloud of trapped atoms in the MOT phase, we use a "Tandem AOM" technique in order to generate a frequency sweep over resonance. All of these tasks make use of acousto-optic-modulators (AOMs) in order to shift the frequency of the light. Some of the electronics needed to drive these devices are also presented.

3.1 Basic Concept

The slowing and trapping of lithium involves four laser frequencies (see the energy level scheme 2-2): For the Zeeman slower, we need light resonant with the hot atoms coming out of the oven (see section 2.4), 1 GHz tuned to the red of the cycling transition. To attain a good loading of the MOT, we want to have approximately 20 mW of laser power available. To prepare the atoms coming out of the oven in the right hyperfine ground state, $F = 3/2$, we provide additional light at the repumping transition, with the same offset of 1 GHz to the red.

For the MOT-beams, we need resonant light at the cycling and at the repumping transition, of equal and possibly high power, with a variable detuning of a few natural linewidths.

The overview of the laser system is given in figure 3-1. It involves one grating stabilized diode laser with about 15 mW output power - the master - and four diode lasers which deliver about 30 mW output power - the slaves - which are frequency-stabilized by injection locking [33, 34]. The master is stabilized to the $2^2S_{1/2}, F = 3/2 \rightarrow 2^2P_{3/2}$-transition in ^{6}Li, with a tunable offset $-\delta$. This is the MOT-frequency used to drive the cycling transition. By the use of three AOMs, we generate light at the repumping transition (+228 MHz from the cycling transition), and at the slower frequencies (-1 GHz from cycling and repumping transition). Each of the slave lasers is seeded with one of these four frequencies. In the following, they are called the "slower", the "slower repumper",

the "MOT" and the "MOT repumper". The MOT and MOT repumper light are overlapped on a polarizing beam splitter cube and coupled into a fiber, as well as the slower and slower repumper beams (the latter with the same polarization, so that clean circular polarized light goes into the slower). Near the vacuum chamber, their light is combined with the yellow sodium light by means of dichroic mirrors.

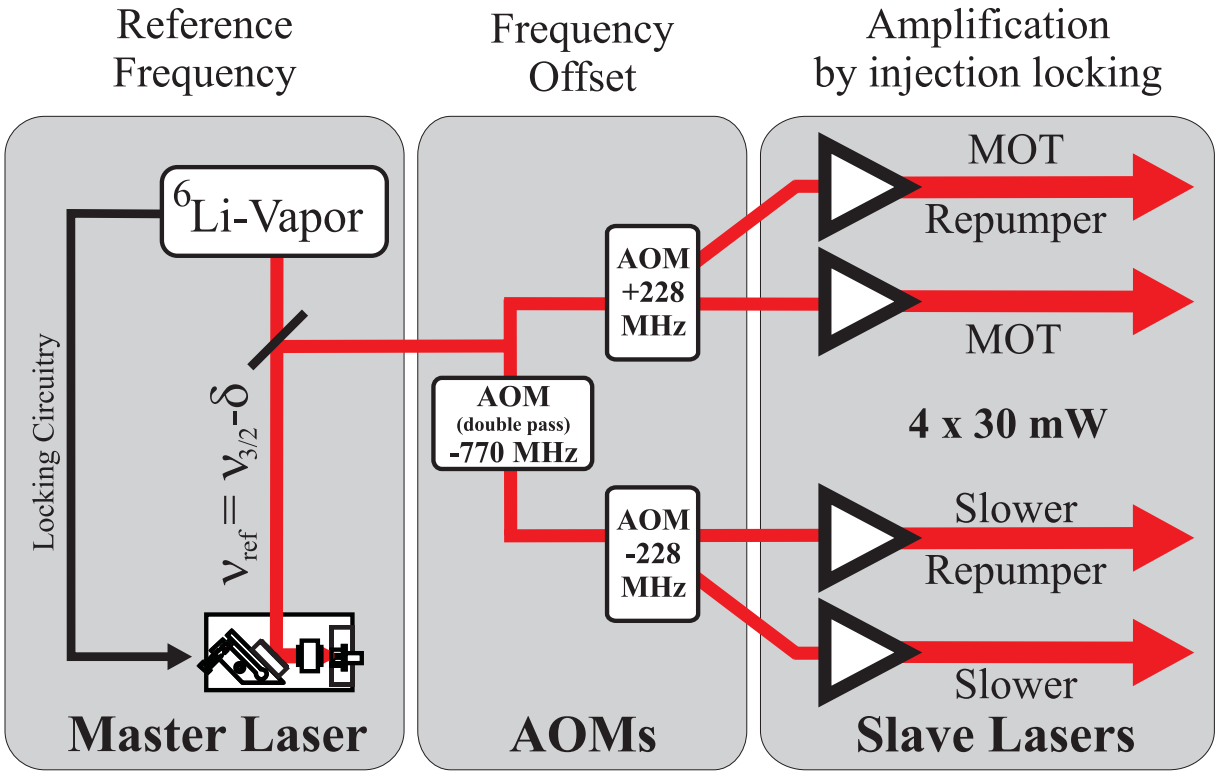

Figure 3-1: *Schematics of the laser system: The master laser is locked to the* $2^2S_{1/2}, F = 3/2 \rightarrow 2^2P_{3/2}$ *resonance line with a tunable offset* $-\delta$*. Three AOMs generate the frequency for the* $2^2S_{1/2}, F = 1/2 \rightarrow 2^2P_{3/2}$ *transition, the repumping light, as well as for the two corresponding frequencies in the slower manifold (shifted by -1 GHz with respect to the MOT and repumper frequencies). This light is then amplified by injection locking of four slave lasers to give an output power of four times 30 mW.*

3.2 Diode Lasers

3.2.1 Free Running Diode Lasers

This section describes briefly the basics of laser diodes. For more details, one may refer to the review article of Wieman and Hollberg [35]. In a semiconductor laser diode, light is generated by sending a current through the active region between the n- and p-layers. This produces electrons and holes which in turn recombine and emit photons. Laser action only occurs when the current exceeds a certain threshold value I_{th}. The laser frequency is primarily determined by the band gap of the semiconductor material, by the junction

temperature and the current density. The diode laser behaves like an amplifying medium with a certain gain profile, whose width is about 15 nm or 10000 GHz. The facets of the laser diode, having a reflectivity of $r = 30\%$ (assuming no coating), form a small cavity, whose finesse is $F = \frac{\pi\sqrt{r}}{1-r} \approx 2.5$ and whose length is on the order of $d \approx 1$ mm. Therefore, the mode spacing (or free spectral range, FSR) of a free running diode laser is $FSR = \frac{c}{2d} \approx 100\,\text{GHz}$, and the width of each mode is $\Delta\nu = FSR/F \approx 25\,\text{GHz}$. The linewidth of the emitted laser light lies typically between 20 and 60 MHz, which is not narrow enough for use in laser cooling experiments.

3.2.2 Grating Stabilization

Setup

Free running laser diodes (we use Mitsubishi ML1016R with an output power of 30 mW) are not stable in frequency, not easily tunable and have a large linewidth. However, with the help of an external resonator it is possible to reduce their linewidth to less than 100 kHz by exploiting the high sensitivity of a laser diode to feedback. The easiest setup is the Littrow configuration, where the external resonator is defined by the rear facet of the laser diode and a grating which is simultaneously used as an output coupler for the laser light, and as frequency selector. Its orientation is such that the first order is reflected back to the chip, whereas the zero order is used as the output beam of the laser system. At a given wavelength λ, the angle for which the incoming beam and the reflected first order beam are superimposed is given by $\theta = \arcsin(\frac{m\lambda}{2})$ where m is the number of lines per unit length of the grating, in our case 2400 lines per mm. Varying the angle therefore tunes the frequency. We use the setup described by Ricci et al. [36], which can be readily purchased by Toptica (former TuiOptics) in the form of their DL100 Laser System (see fig. 3-2).

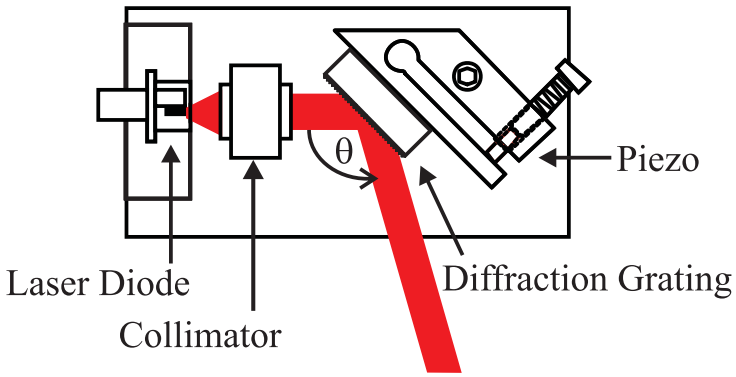

Figure 3-2: *Grating Stabilized Laser System in Littrow Configuration: The external resonator which narrows the linewidth of the diode laser to about 100 kHz is defined by the rear facet of the laser diode and a grating. It serves simultaneously as an output coupler and as a frequency selector.*

Beside the laser itself, this commercial system contains a diode current controller

(TuiOptics DCC 100) and a diode temperature controller. A Diode Laser requires a low noise current and a very stable temperature because current and temperature fluctuations give rise to noise in the emitted frequency. The DCC 100 current controller provides a stability of the current better than 10 μA (DC to 1MHz). The current can be modulated up to 100 kHz. The DTC 100 allows a control of the temperature within 1 mK with long term drifts less than 5 mK.

Operation

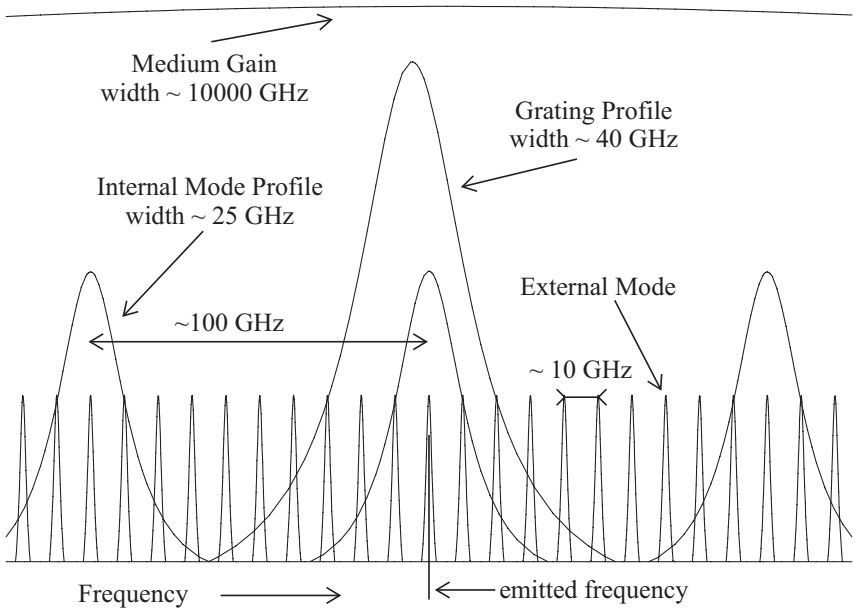

Figure 3-3: *Different gain profiles which all together determine the emitted frequency of a grating stabilized diode laser.*

.

In fig. 3-3 we see the mode structure of the grating stabilized diode laser. The external resonator defined by diode and grating is $L_{\text{ext}} \approx 1\,\text{cm}$ long and therefore has a mode spacing on the order of 10 GHz. The reflectivity of the first order beam in the direction of the chip versus frequency can be regarded as the gain profile of the grating feedback. The quality $\frac{\nu}{\Delta\nu}$ of a grating for a frequency ν is given by the number of lines that contribute to the diffraction. If B is the illuminated length of the grating, only $N = B \cdot m$ lines contribute and we can thus estimate the bandwidth of the grating profile as $\Delta\nu = \frac{\nu}{N} = \frac{c}{Bm\lambda} \approx 40\,\text{GHz}$ for $B \approx 5\,\text{mm}$, the same order of magnitude as the spacing of the internal modes of the diode. By the help of the grating one is therefore able to choose out off those internal modes the one which is needed. The emitted wavelength of the laser is then determined by the point where the medium gain curve, the grating profile, the internal and external cavity modes all roughly overlap as illustrated in fig. 3-3. The linewidth of the emitted frequency is now on the order of 100 kHz [1]. The maximum range the laser

[1]The linewidth of a free-running semiconductor laser is about a factor 50 larger than the Schawlow-

wavelength can be pulled from the medium gain peak by grating feedback is about ± 7 nm.

3.3 Saturated Absorption Spectroscopy of ^{6}Li-Vapor

As an absolute frequency standard the master laser can be stabilized to, one naturally chooses an atomic transition of ^{6}Li. To produce the ^{6}Li-vapor, a ^{6}Li-vapor cell has been built (samples of lithium with an enriched abundance of ^{6}Li are available), in which the metal is heated to 330°C.
In an absorption spectrum of ^{6}Li-vapor at several 100° K, the atomic transition lines are broadened to several GHz by the Doppler effect. Saturated absorption spectroscopy overcomes this problem by selecting out only a specific velocity class of atoms and thus providing Doppler free signals whose width is close to the natural linewidth of the atomic transition ($\Gamma \approx 6$ MHz for the ^{6}Li-D_2 line).

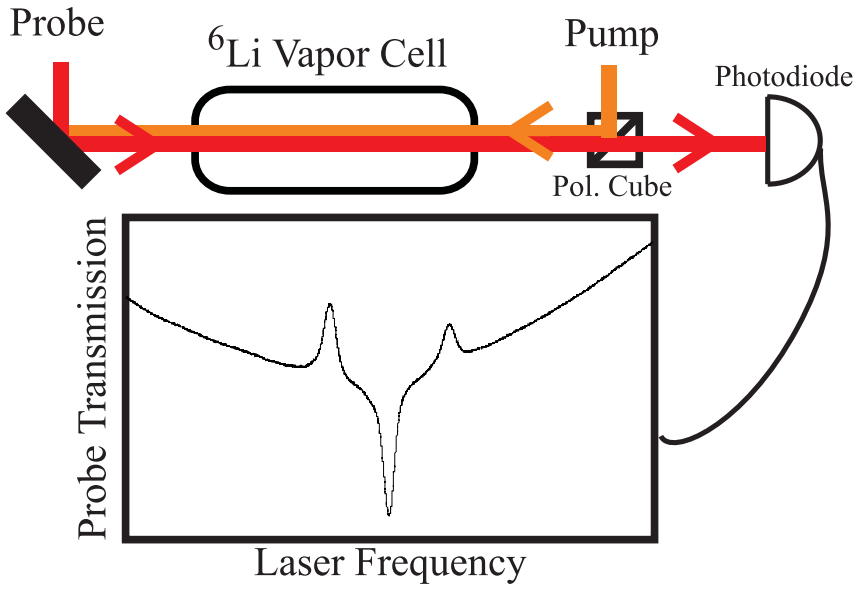

Figure 3-4: *Experimental Setup for Saturated Absorption Spectroscopy: The pumping and the probing beam, overlapped in a ^{6}Li-vapor cell, have the same frequency but opposite directions. The probe beam transmission is detected on a Photodiode (PD). Shown is actual data for the ^{6}Li-D_2 line, discussed in the text.*

The experimental setup for saturated absorption spectroscopy is sketched in fig. 3-4. Two overlapping counterpropagating beams, called respectively the pump and the probe beam, interact with atoms in a ^{6}Li-vapor cell. The probe beam is detected on a photodiode which measures its absorption by the vapor. We suppose here that the probe and the pump beam have the same frequency ν.

Townes limit due to spontaneously emitted photons causing phase fluctuation. The discrepancy is due to a strong coupling between intensity and phase fluctuations in semiconductor lasers [32]. Still, the linewidth depends inversely on the square of the length of the external cavity, leading to the stated linewidth for grating feedback.

The situation for the ^{6}Li-D_2 transition is particularly easy, since the upper hyperfine levels $2^2P_{3/2}, F = \frac{1}{2}, \frac{3}{2}, \frac{5}{2}$ are not resolved (i.e. their distance from each other is less than the natural linewidth of the transition). We can thus regard the atoms as being a three-level system with two ground states g_1 and g_2 and one excited level e, the respective transition frequencies being called $\nu_1 = \omega_1/2\pi$ and $\nu_2 = \omega_2/2\pi$.

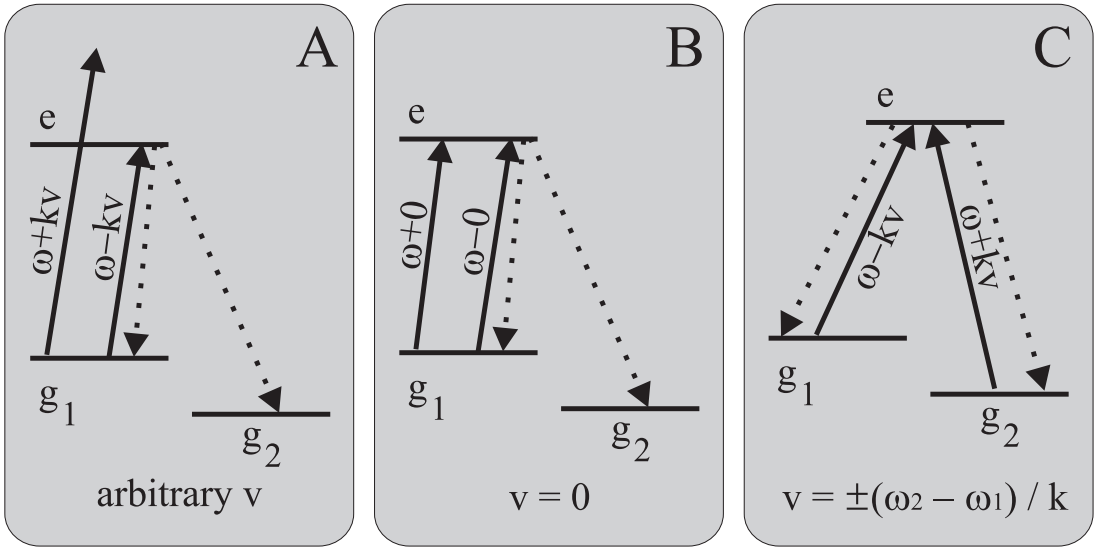

Figure 3-5: *The different cases of saturated absorption spectroscopy in a three-level-system: a) general velocity-class: pump not on resonance at the same time as the probe, whose absorption is not affected, leading to the broad Doppler feature; b) pump and probe resonant with the zero velocity class, the atoms are transferred to the other (dark) ground state, absorption of the probe light is thus reduced; c) cross over: pump excites ground state g_1 (g_2) of atoms with velocity $v = \pm(\omega_1 - \omega_2)/k$, thus populating their ground state g_2 (g_1), which increases absorption of the probe resonant with $g_2(g_1) \rightarrow e$.*

As we can see in fig. 3-5, there are three different cases that together determine the lineshape of the saturated absorption spectrum: Firstly, we get normal absorption of the probe light when the pump is out of resonance for the velocity-class resonant with the probe. This gives the gigahertz-broad Doppler profile. Secondly, if both beams are on resonance with one of the two transitions, the zero-velocity class of atoms gets pumped into the "dark" ground state so that the absorption of the probe light is reduced. And thirdly, if the laser is tuned half way between the two transitions, there are two velocity classes, namely $v = \pm\lambda(\nu_1 - \nu_2)$, for which the pump and the probe are both on resonance with one or the other transition. This way the pump beam will actually increase the population of the ground state that the probe is resonant with, and the probe absorption will be enhanced. This feature is known as the cross-over peak.
The relative strength of each of these features is only determined by the degeneracy of the ground state hyperfine levels. Therefore the dip created by $F = 3/2$-atoms is about twice as large as that of the atoms in $F = 1/2$. The cross-over feature has three times the height as the $F = 1/2$-dip, since six ground state populations contribute to it: The pump beam transfers part of the $F = 1/2$ population of one cross-over velocity class to

$F = 3/2$, and vice versa for the other velocity class. The absorption of the probe light at the cross-over resonance is thus enhanced three times more than it is reduced at the $F = 1/2$-transition.

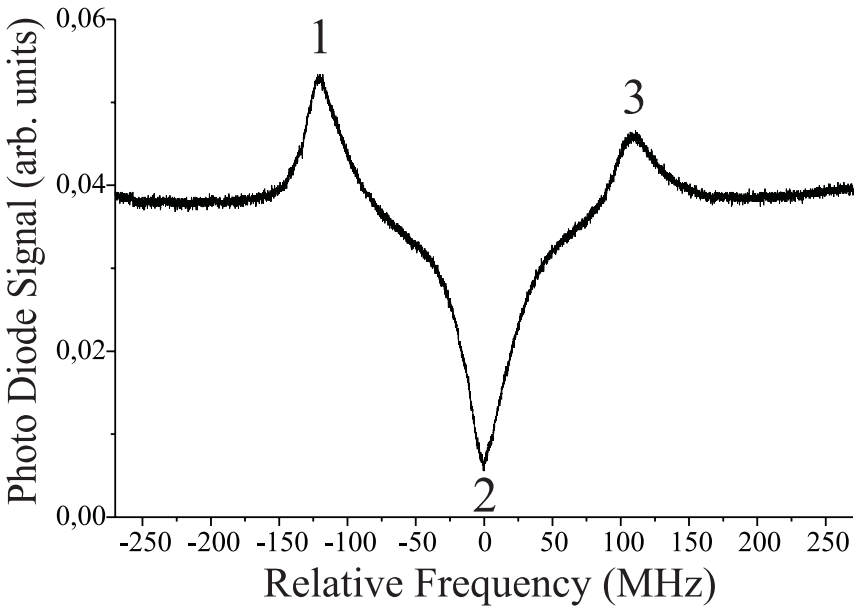

Figure 3-6: *Saturated Absorption Spectrum of the ^{6}Li-D_2 transition (shown is the transmission of the probe beam). 1) denotes the $2^2S_{1/2}, F = 1/2 \rightarrow 2^2P_{3/2}$ transition, 3) the $2^2S_{1/2}, F = 3/2 \rightarrow 2^2P_{3/2}$ transition, 2) is the cross over between those two. It can be seen that the $F = 3/2$ feature is roughly twice as large as the $F = 1/2$ peak, the largest feature being the cross over resonance, as expected.*

In fig. 3-6 the saturated absorption spectrum for the ^{6}Li-D_2 line is shown. It consists of the two Lamb dips separated by 228.2 MHz, the hyperfine splitting of the ^{6}Li ground state $2^2S_{1/2}$, and the cross-over peak in between the two. The width of the features is found to be $\Gamma' \approx 26$ MHz, roughly four times the natural linewidth of lithium, a clear sign of pressure broadening by the buffer gas. Although we did not undertake any quantitative measurements on that effect, by increasing the pressure of the argon buffer gas we could observe in real time the broadening of the spectral lines. The final value of 100 mTorr as the argon pressure was chosen as a trade-off between the pressure broadening and the necessity of avoiding the coating of the glass cell windows.

Since the cross-over is the most pronounced feature in the spectrum, it is the natural choice as frequency standard for the laser stabilization, which will be explained in the next section.

3.4 Frequency Stabilization

3.4.1 Principle

In order to stabilize the master laser to a reference frequency ν_{ref}, one has to create an error signal which is proportional to the deviation of the actual laser frequency $\nu - \nu_{\text{ref}}$, and feed back that signal to the laser. The saturated absorption signal seen in figure 3-6 is symmetric around a resonance frequency and cannot be used as an error signal. When we deviate from the peak's central frequency, we have no information about the direction of that deviation, and whether positive or negative feedback should be applied. The derivative of the saturated absorption spectrum provides this information. So the task is to implement a way of differentiating the spectrum, to set the laser on the largest slope, and to feed back the error signal to the laser.

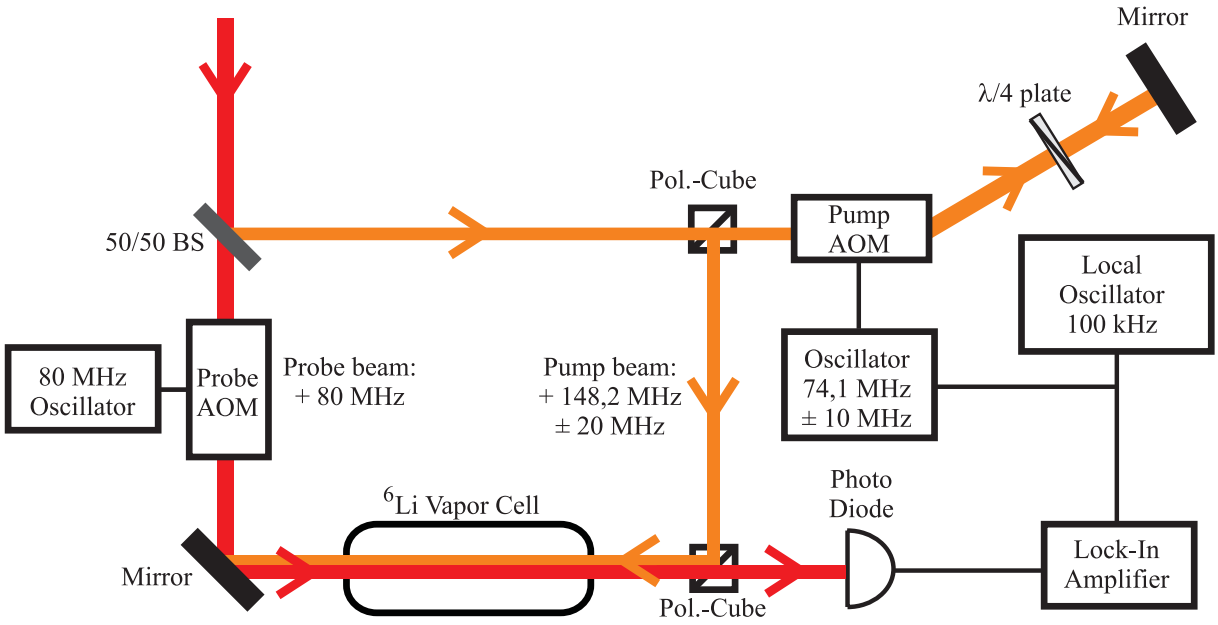

Figure 3-7: *Setup of the frequency stabilization. The frequency of the pump is modulated by an AOM in double pass configuration. The photodiode signal is demodulated by a lock-in amplifier which filters out the Fourier component of the probe beam at the modulating frequency.*

3.4.2 Lock-In Technique

An easy and robust way of solving that task is by using a lock-in technique: As before, the probe beam at frequency ω is detected on a photodiode in the saturated absorption spectroscopy setup. Now we modulate the frequency of the pump beam with the help of an double-pass-AOM according to

$$\omega_{\text{pump}} = \omega + \Delta\omega(t) = \omega + 2\Delta\omega\cos(\omega_{\text{LO}}t),$$

where $2\Delta\omega$ is the amplitude and ω_{LO} the frequency of the modulation (see fig. 3-7). The atoms in the vapor cell will be on resonance with both beams if $\omega = \omega_0 - \frac{\Delta\omega(t)}{2}$, which occurs for atoms in the velocity class $v = -\frac{\Delta\omega(t)}{2k}$ (the minus sign indicates that the atoms fly towards the probe beam). This will therefore shift the saturated absorption peak by $-\frac{\Delta\omega(t)}{2}$. The lineshape $f(\omega)$ detected at the photodiode for the probe will follow that modulation (provided that $\omega_{\mathrm{LO}} \ll \Gamma$):

$$f(\omega) \to f(\omega + \frac{\Delta\omega(t)}{2}).$$

This modulated lineshape is now fed into a lock-in amplifier. This device is essentially a narrow pass filter tuned to the frequency of the signal to be measured, in our case ω_{LO}. In addition to filtering, it also provides gain. Both, the filtering at the signal's frequency and the gain stage, enable one to measure even very small signals, way below the noise level. Technical noise like intensity noise of the laser and 60 Hz electrical noise is filtered out. This is why even with an only faint signal from the saturated absorption spectroscopy ($< 5\,\mathrm{mV}$ at the peak) we are able to produce a large and stable error signal as feedback for the laser-lock.
In mathematical terms, the output of the lock-in amplifier is proportional to the Fourier transform at ω_{LO} of the incoming signal V_{in}:

$$V_{\mathrm{out}} = G\frac{2}{T}\int_0^T \mathrm{dt}\cos(\omega_{\mathrm{LO}}\mathrm{t})\mathrm{V_{in}(t)},$$

where T is the integration time of the filter ($T \gg \frac{1}{\omega_{\mathrm{LO}}}$) and G is the gain. For example, a pure harmonic signal [2] $V_{in}(t) = A\cos(\omega_{\mathrm{LO}}t)$ will result in an output of $V_{\mathrm{out}} = GA$. In our case, the input is just the modulated lineshape $f(\omega + \Delta\omega\cos(\omega_{\mathrm{LO}}t))$, so that the output of the lock-in amplifier is

$$V_{\mathrm{out}} = G\frac{2}{T}\int_0^T \mathrm{dt}\cos(\omega_{\mathrm{LO}}t)f(\omega + \Delta\omega\cos(\omega_{\mathrm{LO}}t)).$$

For $\Delta\omega \ll \Gamma$, we can expand that expression around ω:

$$f(\omega + \Delta\omega\cos(\omega_{\mathrm{LO}}t)) \approx f(\omega) + f'(\omega)\Delta\omega\cos(\omega_{\mathrm{LO}}t).$$

The constant term $f(\omega)$ does not contribute to the integral, but the second term oscillating at ω_{LO} results in an output signal proportional to the derivative of the lineshape:

$$V_{\mathrm{out}} \approx G\Delta\omega f'(\omega).$$

Intuitively, this is what we expect, since by modulating the frequency of the pump beam, one explores the neighborhood of the lineshape around the center frequency ω. Its slope is then found by adding up relative position ($\propto \cos(\omega_{\mathrm{LO}}t)$) times the actual height of the

[2] A possible phase-shift ϕ of the incoming harmonic signal can be brought to zero on the lock-in amplifier.

signal at that position ($f(\omega + \Delta\omega\cos(\omega_{\mathrm{LO}}t))$).

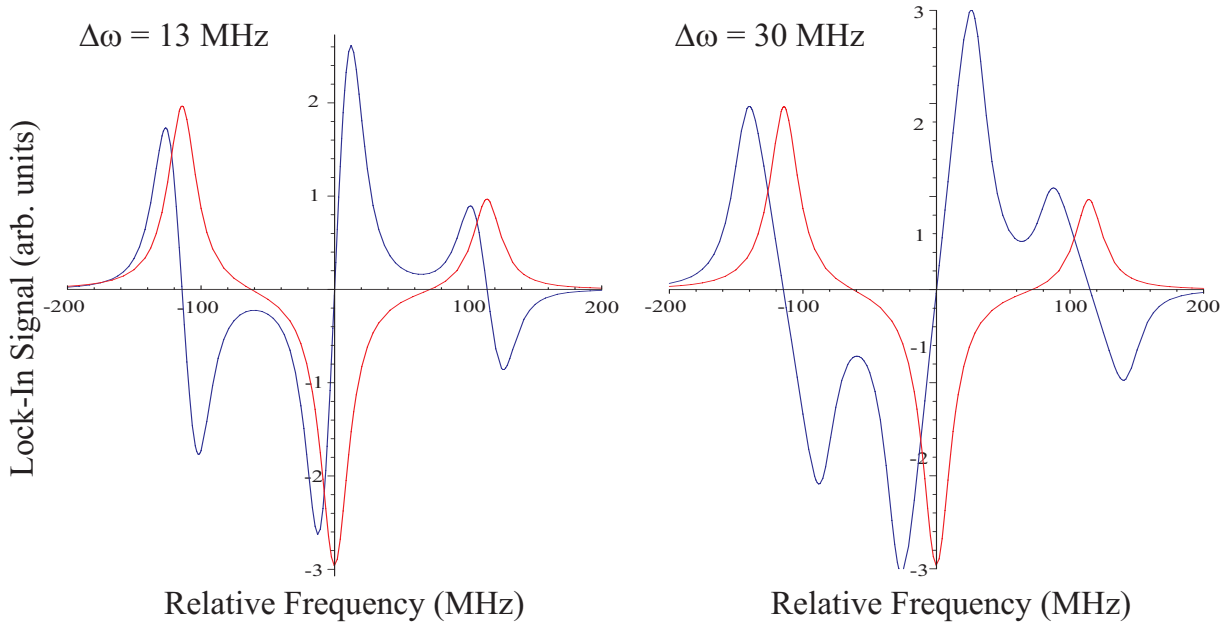

Figure 3-8: *Calculated spectroscopy signal together with the expected locking signal for two different values of* $\Delta\omega$*. On the left we have* $\Delta\omega = 13$ MHz*, on the right* $\Delta\omega = 30$ MHz*, while the linewidth for those curves was taken to be* $\Gamma' = 26$ MHz*, close to experiment. While a value of* $\Delta\omega = \frac{\Gamma'}{2}$ *gives a very good signal with a steep slope, further increase in* $\Delta\omega$ *leads to a degradation in the signals slope and in resemblance to the derivative of the saturated absorption spectrum. The calculations were done using the analytic expression for the lock-in signal found in appendix B.*

In fig. 3-8 we show two calculated lock-in signals for different values of the dithering amplitude $\Delta\omega$. While at first for small amplitudes the signal resembles the derivative of the saturation spectrum and grows with $\Delta\omega$, we see that for amplitudes larger than about half a linewidth the signal's slope starts to degrade and the signal itself is distorted from the former similarity to the derivative. The best choice for $\Delta\omega$ is therefore to be found around $\frac{\Gamma'}{2}$ (where Γ' is the effective linewidth including pressure broadening). A mathematical analysis of the signal's shape can be found in appendix B.

In fig. 3-9 we see the actual error signal produced by the lock-in amplifier. Naturally, the biggest feature with the steepest slope is that of the cross-over resonance, which is 114.1 MHz away from the $2^2S_{1/2}, F = \frac{3}{2} \rightarrow 2^2P_{3/2}$ transition. Since we want the master laser to be on resonance with that transition, with a tunable offset δ, we use AOM's to shift the probe frequency by +80 MHz. The pump frequency is shifted by two times +74.1 MHz + δ (AOM in double pass configuration), plus the modulation $\Delta\omega\cos(\omega_{\mathrm{LO}}t)$. By virtue of the pump beam's double pass AOM, we can easily tune the frequency of the master laser by several tens of MHz, while still being locked.

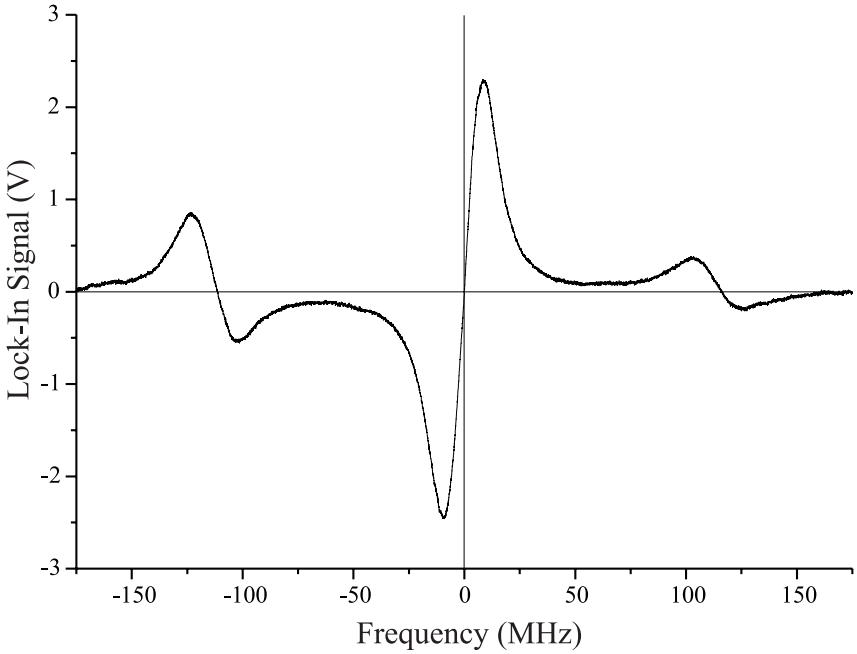

Figure 3-9: *The error signal used to stabilize the laser to an atomic resonance, without any averaging. The width of the central feature is 18 MHz. After locking, the residual rms-noise of the error signal is about 3% of the height of the signal, so that the accuracy of the laser frequency is better than a MHz.*

3.4.3 Electronics

AOM-Driver

Whenever a light frequency shift on the order of a GHz or less is needed, acousto-optic modulators (AOMs) are a common choice. They basically consist of a crystal (e. g. Tellurium Dioxide, TeO_2) with a piezoelectric transducer attached to one of its ends, allowing applied radiofrequency (RF) power to be transformed into a sound wave inside the crystal. The traveling sound wave can exchange energy and momentum with photons traversing the crystal, thus affecting the frequency, direction and intensity of the outcoming laser beam.
We can describe this effect as a Bragg diffraction of photons with wave vector $\vec{k}$ and frequency $\omega = \left|\vec{k}\right| \cdot c_0/n$ and phonons with wave vector $\vec{K}$ and frequency $\Omega = \left|\vec{k}\right| \cdot v_s$. Here c_0 is the light speed in vacuum, n and v_s the refraction index and the speed of sound in the crystal ($v_s = 4260\,\mathrm{m/s}$ for TeO_2). From conservation of energy and momentum it follows for the diffracted photon:

$$\omega' = \omega + \Omega \quad \text{and} \quad \vec{k}' = \vec{k} + \vec{K}$$

Since optical frequencies are about seven orders of magnitude higher than acoustic frequencies, $\Omega \ll \omega$, we have $\left|\vec{k}'\right| \approx \left|\vec{k}\right|$. We can thus deduce from fig. 3-10 the condition

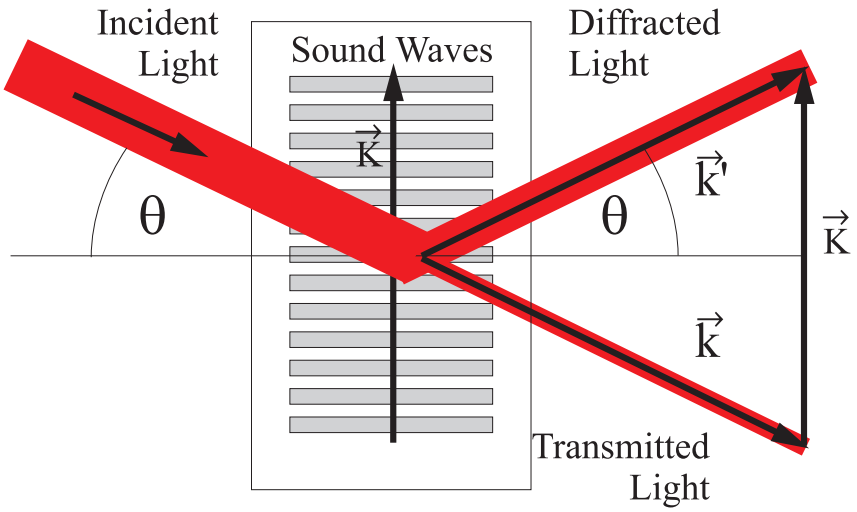

Figure 3-10: *Bragg Diffraction: Sound waves in a crystal partially reflect an incident light beam when the angle of incidence θ satisfies the Bragg condition.*

for Bragg-scattering:

$$\sin\theta = \frac{\vec{K}}{2\vec{k}} = \frac{c_0}{2nv_s} \cdot \frac{\Omega}{\omega}.$$

The efficiency of the first order diffraction first increases with incoupled RF power, but rolls off at a certain point, where two- or multiphoton processes start playing a dominant role. It must be kept in mind that for high-frequency AOMs one can already destroy the crystal before having reached the roll-off point.

The driver which supplies the AOMs with the needed RF Power is sketched in fig. 3-11. The output of a frequency generator which defines the modulating frequency ω_{LO} is added in an analog way to a DC offset voltage and fed into a Voltage Controlled Oscillator (VCO). With the DC offset voltage one can control the detuning of the master laser with respect to the $2^2S_{1/2}, F = \frac{3}{2} \rightarrow 2^2P_{3/2}$ transition. The amplitude of the frequency generator defines the modulating amplitude $\Delta\omega$. When choosing the modulating frequency ω_{LO}, the bandwidth of the VCO has to be respected, which is about 100 kHz. A lower bound is set by the integration time of the lock-in amplifier, which we want to be as low as possible so the laser stabilization can react to fast disturbances. The lowest integration time on the SR510 lock-in amplifier (Stanford Research Systems) is $T = 1\,\mathrm{ms}$, so we choose $\omega_{\mathrm{LO}} = 2\pi \cdot 50\,\mathrm{kHz}$.

PI-Controller

In order to stabilize the frequency of the master laser, the error signal has to be fed back to the laser itself, in order to keep the laser on resonance. A frequency controlling element is the piezo-electric transducer (PZT), which changes the length of the external cavity of the laser. The bandwidth of the PZT is on the order of 1 kHz. Moreover, feedback can be provided to the current of the diode with a bandwidth of about 100 kHz. Several feedback schemes are common: Simple proportional (P) feedback is able to correct relative

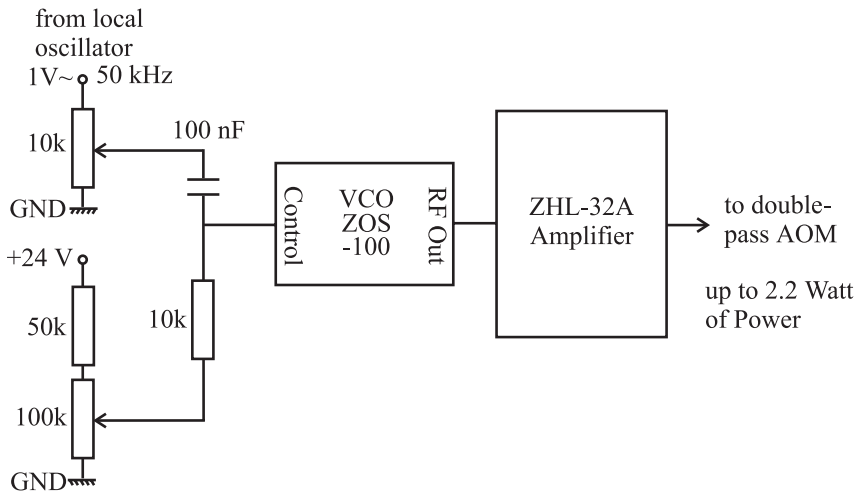

Figure 3-11: *AOM-Driver used for the locking circuit. The modulating signal is added with the help of a high-pass (time constant 1 ms) to the dc offset which sets the center frequency of the AOM.*

deviations, but is never able to zero the error signal, since that would mean zero feedback. An additional integral (I) feedback overcomes that problem: A constant offset from zero charges a capacity whose voltage is fed back to zero that offset. The PI-Controller I built has integral (I) and proportional (P) feedback for the PZT, as well as proportional feedback to the laser current. In our setup, being limited by the integration time of the lock-in amplifier of 1 ms, one does not necessarily need current feedback, but it does nevertheless improve the stability of our laser lock.

The electronic circuit of the PI-Controller can be found in appendix C. To save space, the PI-controller box has been built inside the DL100 Rack, which also provides the supply voltage and connections to the current controller and the PZT voltage.
To lock the laser, we scan the laser frequency, looking at the wavemeter, to find the ^{6}Li-D_2 line. Then, still scanning, we switch on the current feedback and narrow down the scan range at the cross-over feature. The current feedback will already lock the laser, but is not able to zero the error signal, as explained above. After we switch on the integral feedback onto the grating, the laser usually stays locked for the day. The persistent rms-noise on the error signal is about 3% of the height of the 18 MHz wide cross-over feature, which provides an estimate of the accuracy of the laser lock of less than a MHz.

3.5 Creating the MOT-Light

In order to excite the two hyperfine levels of ^{6}Li, we need two laser frequencies separated by 228.2 MHz. The master laser is locked on the MOT-transition ($2^2S_{1/2}, F = 3/2 \rightarrow 2^2P_{3/2}$, with tunable offset), so we use a 228 MHz AOM with 50% efficiency to create the repumper frequency. In addition to the MOT-light, we also need the slowing light, red-detuned by 1GHz with respect to the MOT-manifold. To connect the two manifolds, we use a 380

MHz-AOM in a double pass configuration. This setup allows us to change the slower frequency without misaligning the beams. In a double pass, the first diffracted order of the AOM is back reflected into the crystal. The first diffracted order of the back reflected beam then perfectly overlaps with the incoming beam, independent of the AOM frequency. To couple the beam out, one places a $\lambda/4$ wave plate in front of the back-reflecting mirror. This rotates the polarization of the back reflected beam by 90°. A polarizing beam splitter cube couples the beam out. A complete but rather technical drawing of the laser system can be found in appendix A.

The frequency after the double pass is the repumper for the slower manifold, shifted 760 MHz to the red of the master's frequency. Another 228 MHz AOM in single pass, and adjusted to 50% efficiency, creates the actual slower frequency at about -1000 MHz with respect to the master. In that way, all four frequencies have been created, all being equal in power (adjusted by a combination of a $\lambda/2$ wave plate and a polarizing cube), and ready to be seeded into the slave lasers with the help of four Faraday Isolators (see section 3.6).
We use anamorphic prism pairs to shape the elliptic beams emitted from the slave laser diodes into round beams 5 mm in diameter. The MOT and MOT repumper beams are overlapped on a polarizing beam splitter cube, as well as the slower and slower repumper beams. The intensity of each beam can be chosen by means of a $\lambda/2$ wave plate. Two telescopes couple the MOT and slower light into two fibers that lead to the experiment. In the focus of those telescopes we place shutters to switch off the light after the MOT-phase. Near the vacuum chamber, the MOT-light for lithium and sodium are overlapped by means of dichroic mirrors.

3.6 Amplification by Injection Locking

Our grating stabilized diode laser gives an output power of 15 mW. This is not sufficient for capturing a large number of atoms in the MOT. More laser power at the desired frequencies can be obtained by coupling narrow-band light from the grating stabilized diode laser, the master, into a free running diode laser, the slave, by means of an optical isolator (see fig. 3-12). The free running diode is thus forced to emit light at the same wavelength and with the same narrow linewidth as the injected light, but with the intensity of a free running laser [33].

The diodes used in the slave lasers happen to have their free running wavelength at room temperature around 665 nm. In order to pull them near the desired frequency we have to heat the diodes to around 50°C, at which point their free running wavelength is around 668 nm. Heating the diodes is not desirable, since it shortens their lifetime considerably, but it is unavoidable.
The alignment procedure for injection locking is as follows: During the whole procedure, we observe the spectral output of the slave laser with a spectrum analyzer (Fabry-Perot). First, the seeding beam is brought to enter the optical isolator such that it roughly hits the collimating lens of the slave. The diode current of the slave is then reduced close to the threshold current. For further alignment we make use of the fact that a small part

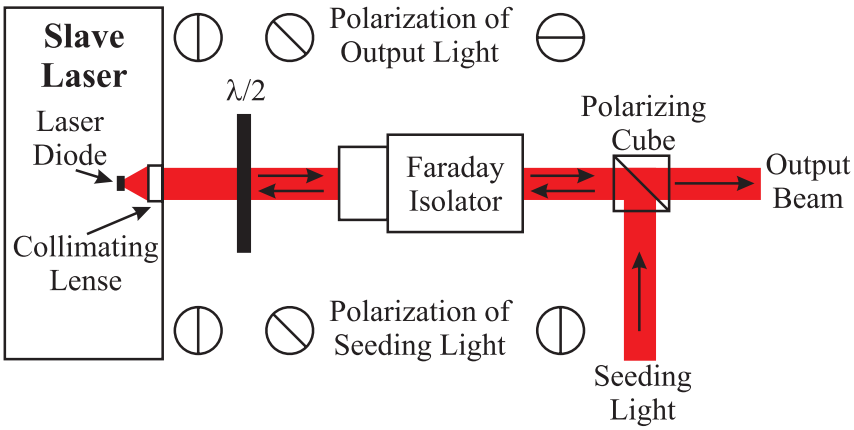

Figure 3-12: *Principle of Injection Locking. The different polarizations of both the seeding light and the output beam are sketched. The slave laser emits light at the same frequency and with the same narrow bandwidth as the seeding light coming from the master.*

of the seeding light is actually back-reflected from the diode housing and can thus be seen near the output beam of the slave laser. As for the grating feedback, a sign of a good injection lock is a lower threshold current. When the back-reflected beam of the seeding light is well overlapped with the slave's output beam, one can see the slave beam brighten up as a result of the lowered threshold current. At this point one can already see the narrow peak in the Fabry-Perot spectrum (see fig. 3-13) in addition to the broad free-running spectrum: Some of the slaves laser power is already emitted in the desired mode. By fine aligning the mirrors and adjusting the diode current one transfers finally all the power in this peak. For every slave laser we use approximately 1 mW of master power for the seeding.

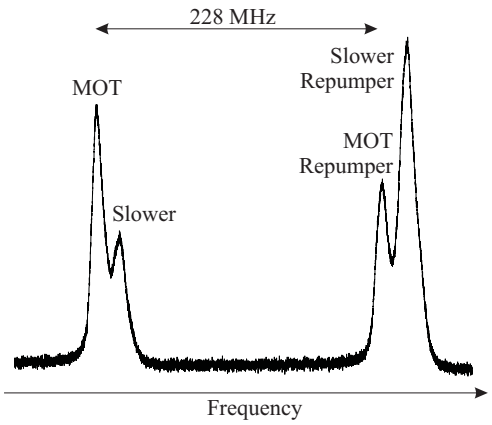

Figure 3-13: *Slave Laser Monitor. All Slaves are observed at the same time in a Fabry-Perot cavity, having a mode-spacing of 1 GHz and a linewidth of 10 MHz. The slower is roughly 1 GHz tuned to the red of the MOT-frequency, therefore their cavity modes are close to each other.*

3.7 Imaging Light

The easiest way to image the trapped atoms in the MOT is just by taking a picture of their fluorescence light. For more quantitative analysis of the atom cloud and of course for imaging it in the magnetic trap with all lights switched off, one rather uses absorption imaging: The shadow cast by the atoms absorbing resonant light is recorded onto a CCD camera chip. This is how all the data on the atomic sample is taken. In addition to that, one also likes to have an absorption monitor, a beam whose frequency is scanned over resonance while it is sent through the clouds of atoms and detected by a photodiode. The measured absorption signal can be used for a rough estimate of the number of atoms in the MOT and is therefore useful for tweaking the MOT-beams.

Tandem AOM Technique

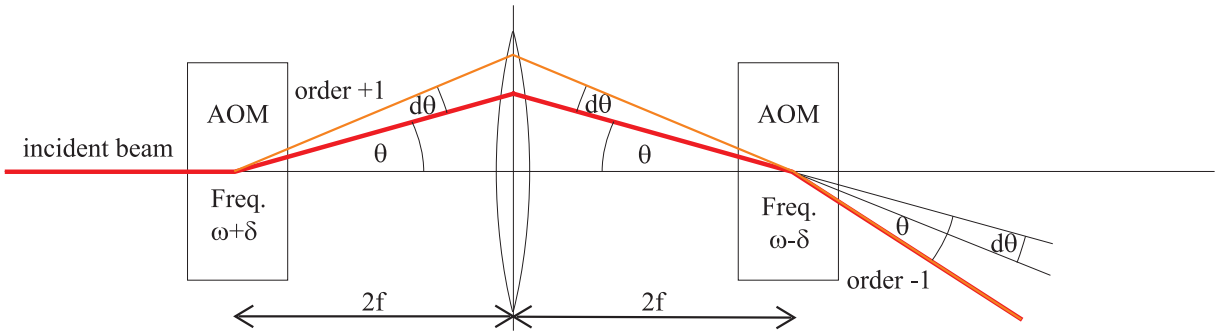

Figure 3-14: *Schematics of the Tandem AOM Setup: A first AOM driven at frequency $\omega + \delta$ deflects the incident beam in first order by an angle $\theta + d\theta$, a lens maps this beam onto the second AOM which is driven at frequency $\omega - \delta$. The direction of the minus first order beam coming out of the second AOM is constant, independent of δ, and is shifted in frequency by $(\omega + \delta) - (\omega - \delta) = 2\delta$ with respect to the original beam.*

Both tasks, creating the resonance frequency and the frequency sweep, can again be solved by the use of AOMs. We need actually two AOMs in the so-called "Tandem configuration" to be able to produce a frequency sweep without moving the beam. The light for this probe scan is taken out of the MOT-light, which is near resonance to the $2^2S_{1/2}, F = 3/2 \rightarrow 2^P_{3/2}$ transition.

The schematics are shown in fig. 3-14: The incident beam traverses the first AOM, driven at frequency ω, and is deflected by an angle θ in first order Bragg diffraction. A lens, placed in the middle between both AOMs, such that its distance from each crystal is twice its focal length, images the beam in the second AOM, which is driven at the same frequency as the first. The minus first order beam of this AOM is thus deflected by a total angle 2θ from the original beam, whereas its frequency has not changed. If the frequency of the first AOM is now changed by an amount δ, and at the same time the second AOM by $-\delta$, the additional deflection angle $\Delta\theta$ after the first AOM is compensated for at the second AOM, so that in total the outcoming beam has not changed its direction. Its

frequency though has changed by a total of 2δ. This is how a frequency sweep can be accomplished without stirring the beam, so that it can actually be coupled into a fiber and brought to the experimental table.

The Tandem AOM Driver I built for this task is sketched in fig. 3-15. Rather than applying two voltages $V + d$ and $V - d$ to two different Voltage Controlled Oscillators (VCOs), which will certainly have a slightly different frequency-to-voltage response, we use three VCOs at 600 MHz, 800 MHz $+\delta$ and 1000 MHz and take the difference frequency to create RF power at 200 MHz $\pm\delta$. This has the additional advantage of a large accessible frequency range. Therefore there are three input voltages, one for each of the VCOs. Two of them are fixed (only adjustable inside the driver box), whereas the middle one can either be set to a constant voltage (by example to produce resonant light for imaging) or be controlled externally to allow a frequency sweep with the help of a frequency generator. Which of the two options is in use is determined by an analog multiplexer, controllable either manually or by the word-generator that governs the timing of the experiment [3]. The output of the center VCO is compared with the two side frequencies by a mixer which outputs the difference frequency [4]. The power for both difference frequencies can be adjusted by means of an electronic attenuator, for one of which external control is also available. This allows for intensity stabilization during the frequency sweep. That is necessary since neither is the output power of the RF-electronics independent of the frequency, nor are the tandem AOMs perfectly set up, so that the output efficiency varies during the frequency sweep. For a very fast switching of the imaging light, two TTL-switches are built in. The remainder of the circuit amplifies the signal from a little less than a mW up to the final power of 1 W.

Intensity Stabilization

As stated before, intensity stabilization is needed to keep the light level constant during the frequency sweep. For that purpose, a photodiode measures the probe beam's intensity after it leaves the fiber near the vacuum chamber. In this way also fluctuations in the fiber are compensated by the stabilization. The diode's signal is compared to a set value by a differential amplifier (see fig. 3-16), whose output is then amplified and integrated in a PI-Controller, and fed back to the tandem AOM driver to deliver the appropriate current to the electronic attenuator. Fig. 3-17 shows the setup at work. The intensity stabilization circuit is found in appendix C.

[3] For instance, we usually like to have the absorption monitor on during the MOT loading phase, and then to switch to resonant probe light to image the atoms.

[4] Since a mixer actually multiplies two signals, we get the difference and the sum frequency, due to the formula $\cos(w) \cdot \cos(v) = 1/2\cos(w+v) + 1/2\cos(w-v)$. Therefore, a low-pass filter selects out the difference frequency).

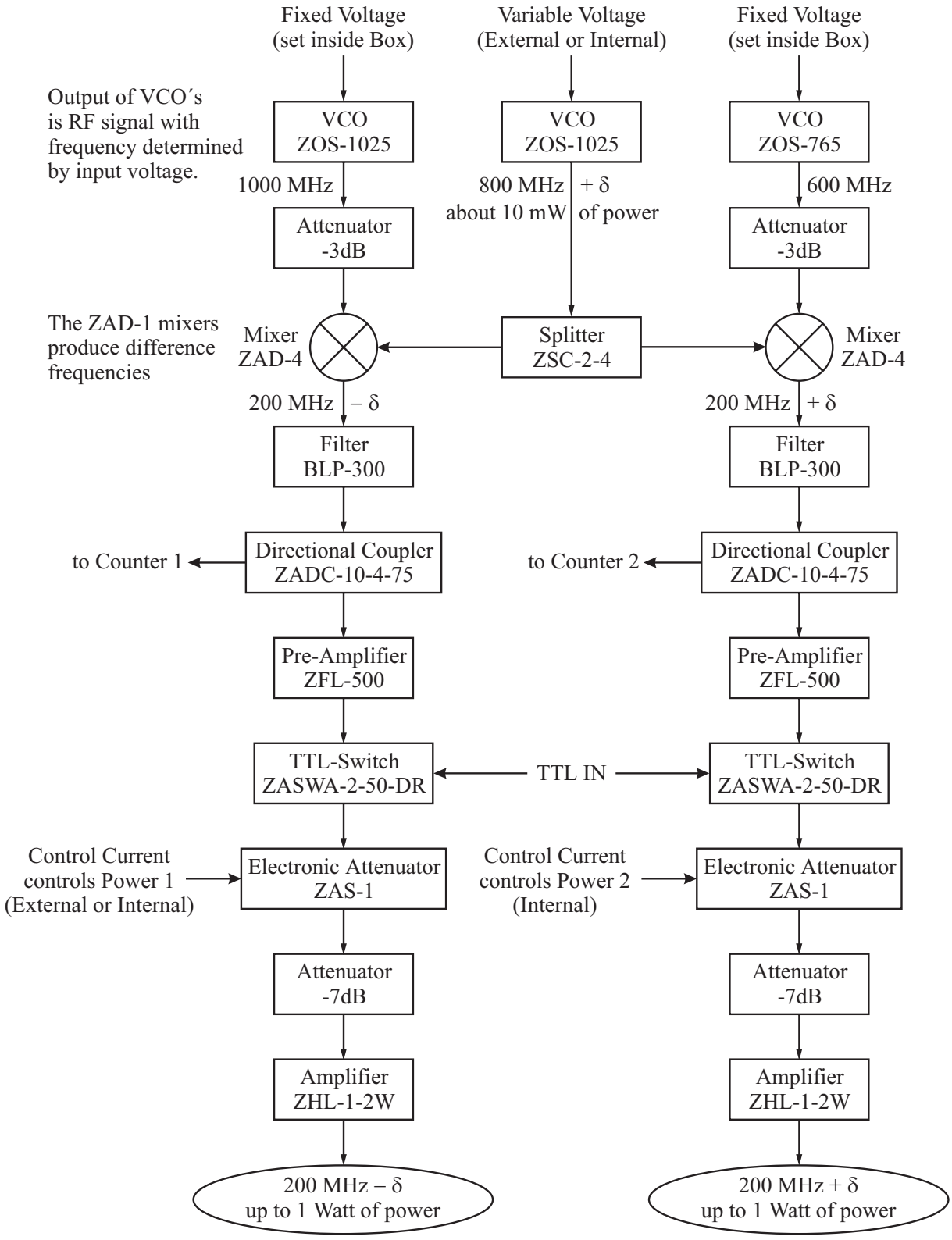

Figure 3-15: *Driver for the Tandem AOM. Two Voltage Controlled Oscillators (VCO) at fixed frequency generate RF-power at 600 and 1000 MHz, a third can be controlled either manually or by an external voltage, to produce RF-power around 800 MHz. A mixer generates the difference frequencies between the variable and the fixed VCOs. The remaining devices are used to control, switch and amplify the output power of the two mixers.*

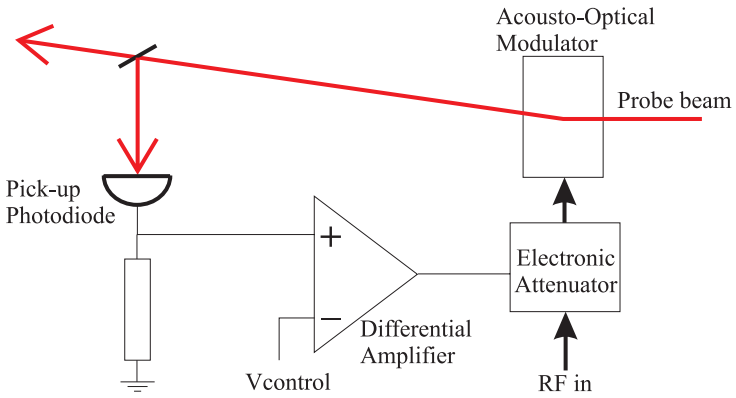

Figure 3-16: *Principle of intensity stabilization. The actual beam intensity is compared to a set voltage. The outcome is fed into an electronic attenuator which controls the RF power of an AOM.*

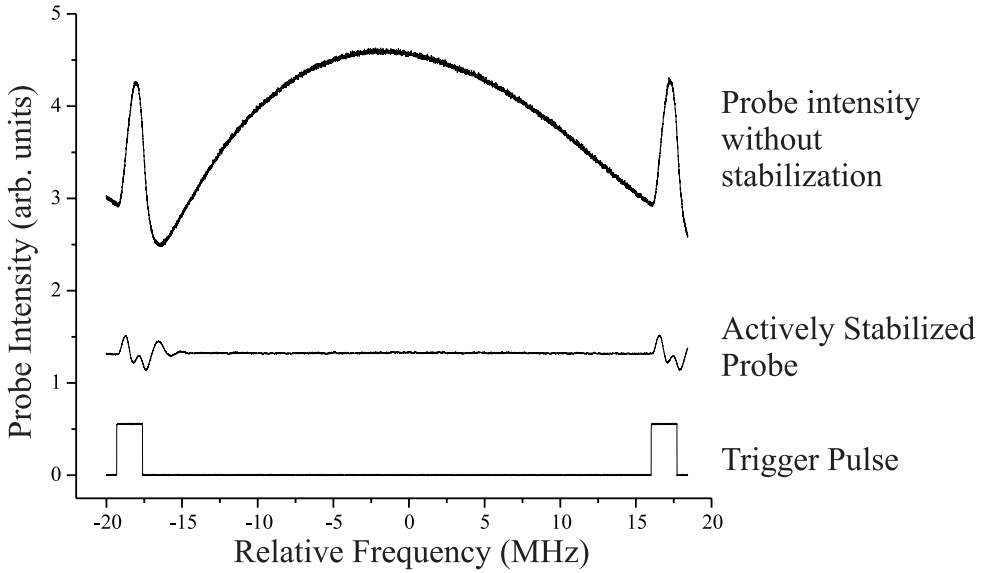

Figure 3-17: *Probe intensity with and without intensity stabilization during a frequency sweep. A 30 MHz frequency range is swept in about 10ms.*

Chapter 4

Double Species Experiment with Sodium and Lithium

In this chapter we report the achievement of a double species MOT of ^{6}Li and ^{23}Na. The atoms are produced in a double species oven, both species are slowed in a Zeeman slower optimized for sodium and captured in a MOT produced by resonant laser light at 589 and 670 nm. The number and temperature of trapped atoms is about 10^{10} at $\approx 1000\ \mu$K for sodium and up to 10^8 at $\approx 600\ \mu$K for lithium.

4.1 The Apparatus

The apparatus for the double-species experiment with ^{23}Na and ^{6}Li has been created by adding the components to create a ^{6}Li-MOT to an existing sodium BEC machine. The methods to create BEC of sodium in this machine has been discussed in detail in [38]. To extent the apparatus, a double species oven has been attached to the sodium-optimized Zeeman slower, creating two collinear atomic beams for sodium and lithium (fig. 4-1), and the light created by the ^{6}Li-laser system has been overlapped with the yellow sodium light. In the case of the slower light, this was accomplished using dichroic mirrors. For the MOT-beams the overlap was achieved on a polarizing cube.

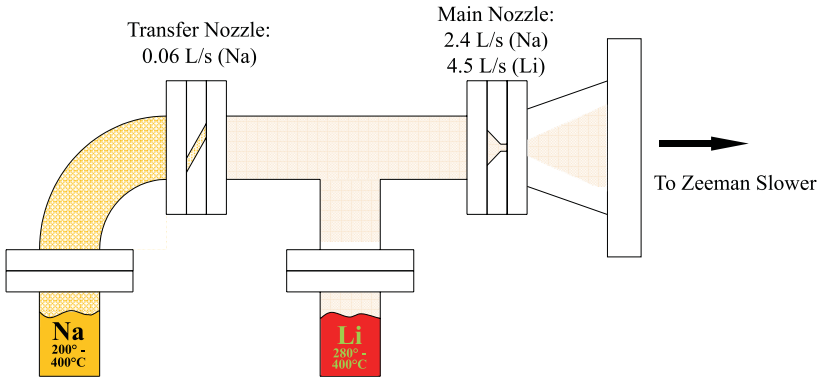

Figure 4-1: *The double species oven used to produce the atomic beam.*

4.2 Imaging the Atoms

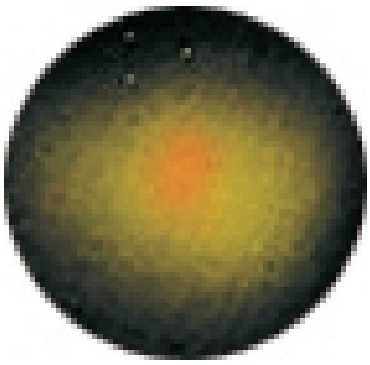

Figure 4-2: *Picture of the double species MOT as seen by the naked eye. The intensity of the sodium-resonant light had to be reduced drastically to produce a sufficiently small MOT so that the fluorescence of the lithium atoms can be seen.*

Absorption Monitor

A reliable value for the number of atoms may be obtained by measuring the absorption of a resonant laser beam passing through the atoms. For that purpose, we sweep the frequency of the probe beam around resonance by the tandem AOM technique described in section 3.7 and detect it on a photodiode. The result is shown in fig. 4-3. To derive the number of atoms from the measured peak absorption, let us suppose a Gaussian-like distribution n of atoms in the cloud. For resonant light, the scattering cross-section [1] seen by unpolarized atoms is $\sigma_0 = \frac{1}{\pi}\lambda^2$. The probability that a photon is absorbed while it travels a distance dz through the cloud is $n\sigma_0 dz$. Therefore we find for the intensity I of a light beam passing through the atoms: $dI = -In\sigma dz$ which results in

$$I(z) = I(0)e^{-\sigma_0 \tilde{n}(z)},$$

where $\tilde{n}(z) = \int_0^z n \cdot dz$ is the integrated column density. Knowing the resonant absorption $\frac{I_{\mathrm{res}}}{I(0)}$ of the cloud gives its optical density $D = \sigma_0 \tilde{n}$. This, multiplied by the apparent (x,y)-area A of the MOT leads to an estimate for the number of atoms:

$$N = \int_V n\, dV = \tilde{n}A = -\frac{A}{\sigma_0} \ln(\frac{I_{\mathrm{res}}}{I(0)}).$$

For fig. 4-3, which was obtained using $2^2S_{1/2}, F = 3/2 \rightarrow 2^2P_{3/2}$ resonant light, $\frac{I_{\mathrm{res}}}{I(0)} \approx 35\%$. The area of the cloud was determined by fitting a 2D-Gaussian in a fluorescence

[1] for a two-level system, it is $\tilde{\sigma}_0 = \frac{3}{2\pi}\lambda^2$. For a multi-level system, we have to sum the respective transition strengths over the possible final states and average over the ground state Zeeman sublevels. In ^{6}Li, the upper hyperfine levels are unresolved, so all of them have to be included in the sum. In conclusion, the averaging over the Zeeman sub-levels for both the $F = 1/2$ and the $F = 3/2$ ground state results in a transition strength 2/3 as strong as for a two-level system.

image of the MOT which gave $A = 4.4\,\mathrm{mm}^2$. Therefore, we get $N \approx 3.3 \cdot 10^7$ atoms in the $F = 3/2$ hyperfine ground state. For $2^2S_{1/2}, F = 1/2 \rightarrow 2^2P_{3/2}$ light we get roughly half the number of atoms, as expected from the degeneracy of the two ground states.

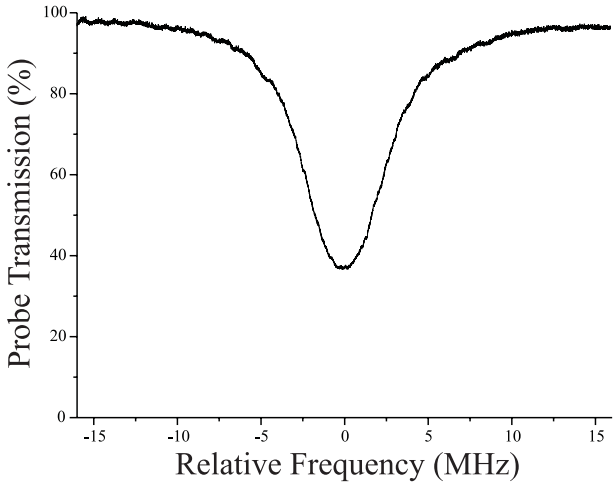

Figure 4-3: *Absorption Monitor of the Lithium MOT. A laser beam, scanned across $F = 3/2$-resonance, is sent through the cloud of atoms captured in the MOT. We record the transmission of the beam on a photodiode. On resonance, transmission is reduced to $\approx 35\%$. The data was taken using the frequency scan method described in section 3.7.*

Absorption Imaging

To go a step further, one images the transmission of a resonant probe beam passing through the cloud onto a CCD camera as described in [38]. Thereby the cloud casts its shadow onto the chip by absorbing the probe light, giving rise to a measured intensity (disregarding noise) of

$$I(x, y) = I_0(x, y)e^{-D(x,y)} + N(x, y),$$

where $I_0(x, y)$ is the probe beam intensity without atoms, $N(x, y)$ is the dark field with no atoms and no probe beam, and $D(x, y) = \sigma_0 \tilde{n}(x, y)$ is the optical density of the cloud, from which the column density $\tilde{n}(x, y)$ can be derived. Since the beam profile is typically far from Gaussian and background light reduces the image quality further, one has to take three images: The probe beam with atoms, giving $I(x, y)$, a bright-field image without atoms, giving $I_0(x, y) + N(x, y)$, and a dark-field image with no atoms and no probe light, which measures $N(x, y)$ (see fig. 4-4, a)-c)). Subtracting the dark field from the first two images and dividing the image with atoms by the bright-field image gives

$$T(x, y) \simeq e^{-D(x,y)}.$$

From that we can again deduce the total number of atoms in the cloud by summing the optical density over the whole image:

$$N = \frac{A}{\sigma_0} \sum_{\text{pixels}} -\ln(T(x,y)),$$

where A is the imaged area per pixel.
In fig. 4-4, which was taken with $F = 3/2 \rightarrow F' = 1/2, 3/2, 5/2$ resonant light, we count an atom number of $N = 3 \cdot 10^7$.

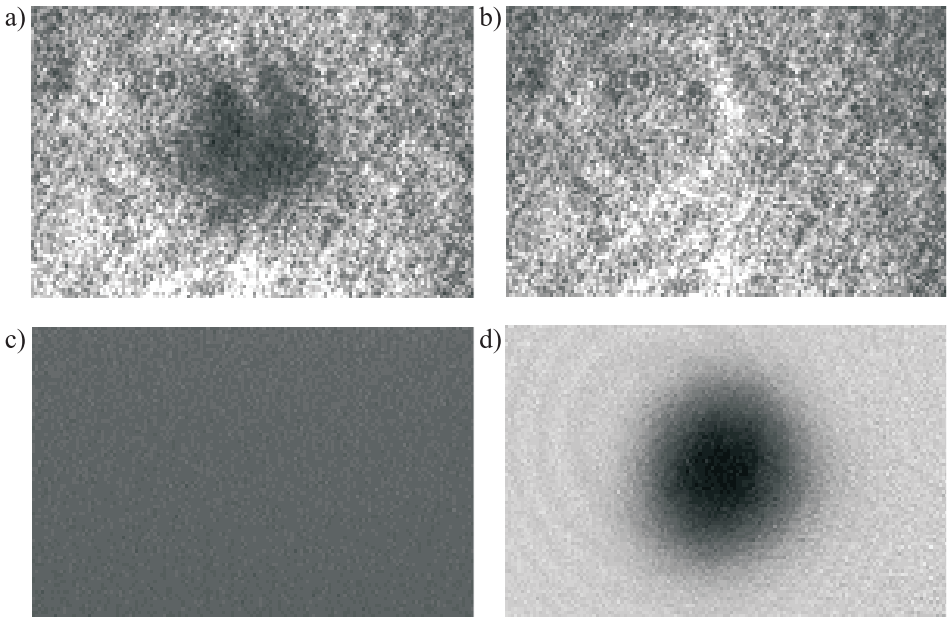

Figure 4-4: *Absorption Image processing. In a), we see the probe light with atoms, the shadow cast by the absorbing cloud is visible but heavily distorted by the inhomogeneous beam profile. In b), an identical image is taken without the atoms, c) shows the dark field without atoms and without the probe light, and in d) we see processed absorption image. For c), a compressed grey-scale was used, since on the same scale as a) and b), the dark field would be completely black. The field of view is 6.6 mm x 3.9 mm.*

4.3 Temperature Measurement of the ^{6}Li-MOT

To characterize the trapped atom cloud further, its temperature may be measured using absorption imaging. After 5 s of loading, the trap light and the quadrupole magnetic field is switched off in about 50 μs at time t_0. Subsequently, we let the cold cloud ballistically expand for a variable time of flight t. Assuming an initial Gaussian density distribution, the 1/e-radius of the cloud increases according to

$$r_{1/e} = \sqrt{r_{1/e}^2(t_0) + \frac{2k_B T}{m}(t - t_0)^2}, \tag{4.1}$$

where m is the mass of a ^{6}Li-atom and T the temperature of the cloud. By repeatedly producing clouds and imaging them after different times of flight, the expansion of the cloud can be followed. The 1/e-radius is determined from a two dimensional Gaussian fit to the absorption profile as shown in fig. 4-6. From a best fit of the data to equation 4.1 the temperature can be deduced.

In fact, this procedure results in two values for the temperature, one for the radial and one for the axial expansion of the MOT (radial and axial defined by the quadrupole coils creating the magnetic field). There is no reason for both values to be exactly equal. The heating rate arising from spontaneous emission is of course isotropic, but the cooling rate for each direction depends on the beam intensity in each of the MOT-arms which can slightly differ [16]. Elastic collisions between the atoms can be neglected, the collision rate being on the order of 10 Hz whereas the cooling rate is given by the molasses damping time, on the order of μs.

4.3.1 Temperature vs. Detuning

The goal of large but at the same time very cold clouds of atoms in a MOT is not easy to achieve [39]. For the steady-state of a MOT, the two goals contradict each other: A large detuning ($\approx -4\Gamma$) and strong laser power lead to a large capture range of the MOT and thus to a high atom number ($\approx 10^8$), but at the same time the temperature increases (> 1 mK). At low detuning ($\approx 1 - 2\Gamma$), the tight confinement leads to small but cold (around 350 μK) ensembles of atoms. The way out of this dilemma might be to first collect a large number of atoms at comparatively large detunings of several Γ below resonance, and then drastically reducing the intensity of the MOT beams for a short time to attain lower temperatures [37]. In order to quantify the behaviour of our ^{6}Li-MOT for different detunings, some additional temperature data has been taken, which is presented in fig. 4-5. It shows that the lowest temperatures can be obtained for $-\delta \approx 2.5\Gamma$. This is in good agreement with the results of [39]. However, the atom number at this point is eight times smaller than for -4.5Γ detuning.

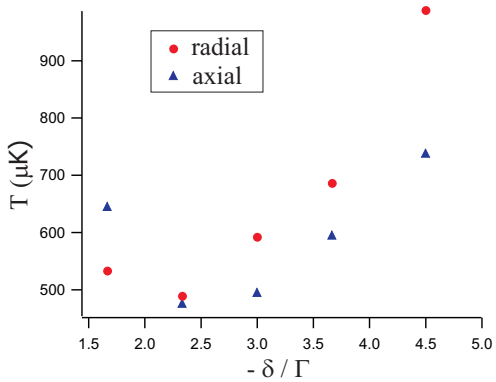

Figure 4-5: *Temperature T as a function of laser detuning in axial and radial direction. The lowest temperature is achieved for $\delta \approx -2.5\Gamma$. However, the number of atoms was eight times smaller than for $\delta \approx -4.5\Gamma$.*

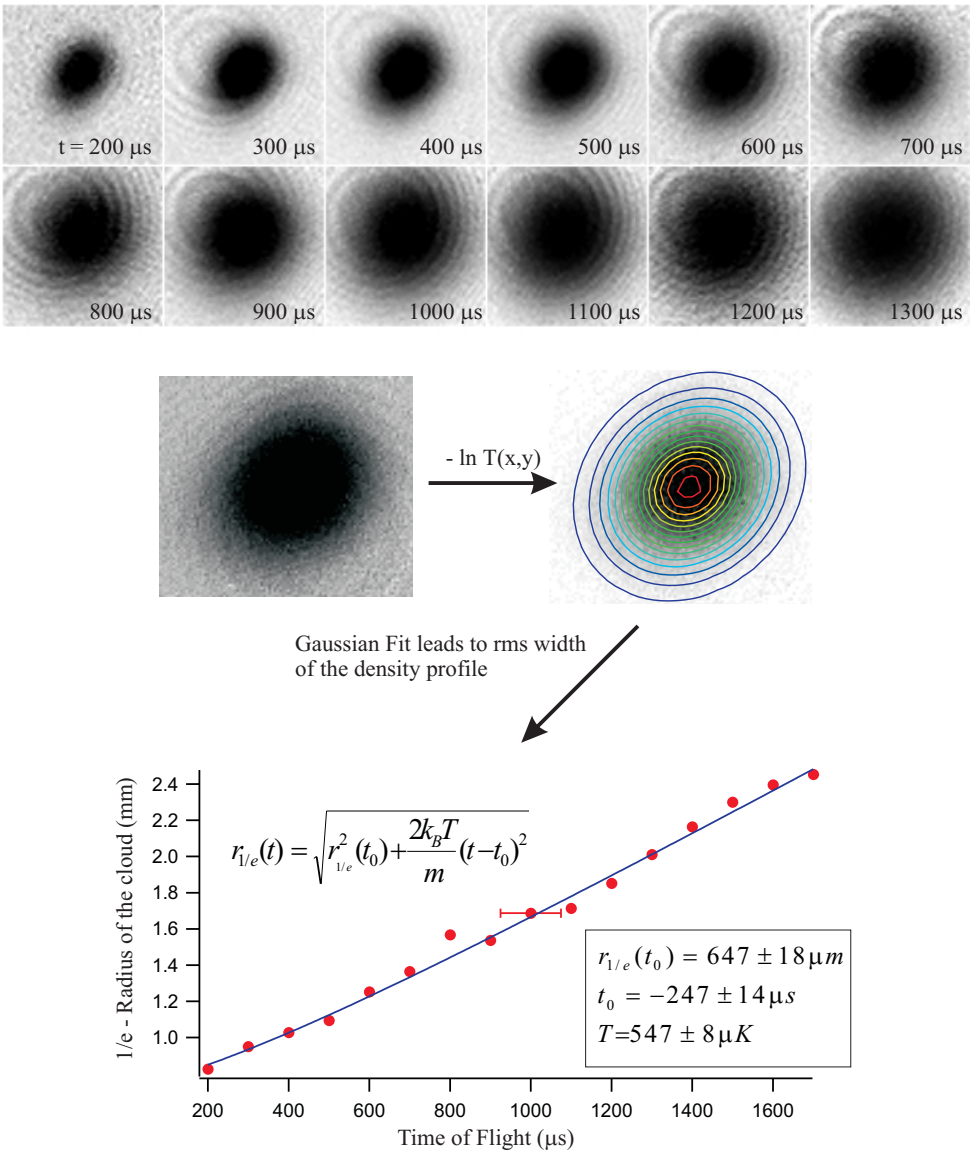

Figure 4-6: *Temperature measurement of the trapped atom cloud. A series of absorption images is taken after a variable time of free expansion of the cloud. To get the optical density, one takes the logarithm of each image. The radial and axial (with respect to the curvature coils of the MOT) 1/e-radius of the density profile is obtained using a two-dimensional Gaussian fit. These radii are plotted with respect to time of flight and the temperature calculated using the above fit-function.*

4.4 The Lithium MOT in the presence of sodium

To estimate the order of magnitude of collisions between sodium and lithium, one can study how the loading of the lithium MOT is affected by the presence of sodium. The main process that leads to atom losses in the MOT is radiative escape, as described in a recent review [42]. Other mechanisms may contribute to the trap losses, for instance fine-structure change and hyperfine change collisions.

We measured the loading and the decay of the Li MOT with and without sodium by imaging the fluorescence of the cloud onto a photodiode. For low densities of atoms, this signal is proportional to the atom number in the MOT. This can be used to get a first estimate on the overall cross-section between Li and Na.
The loading behaviour of Li in presence of Na is given by the rate equation [43]:

$$\frac{dN_{\mathrm{Li}}}{dt} = L - \gamma_0 N_{\mathrm{Li}} - 2\beta' \frac{n_{0,\mathrm{Na}} n_{0,\mathrm{Li}} N_{\mathrm{Li}} N_{0,\mathrm{Na}}}{\left((N_{0,\mathrm{Na}} n_{0,\mathrm{Li}})^{\frac{2}{3}} + (N_{\mathrm{Li}} n_{0,\mathrm{Na}})^{\frac{2}{3}} \right)^{\frac{3}{2}}},$$

where β' is the cross-section between Na and Li, L is the loading rate, γ_0 the loss rate without Na, N_{Li} the number of Li atoms, $n_{0,\mathrm{Li}}$, $n_{0,\mathrm{Na}}$ the densities without the other cloud, $N_{0,\mathrm{Na}}$ the number of Na atoms without Li. Using the estimated volumes of both clouds without the other being present, $V_{\mathrm{Na}} \approx 0.1\mathrm{cm}^3$, $V_{\mathrm{Li}} \approx 0.01\mathrm{cm}^3$, we have $\frac{N_{0,\mathrm{Na}} n_{0,\mathrm{Li}}}{N_{\mathrm{Li}} n_{0,\mathrm{Na}}} = \frac{V_{\mathrm{Na}}}{V_{\mathrm{Li}}} \frac{N_{0,\mathrm{Li}}}{N_{\mathrm{Li}}} = 10 \frac{N_{0,\mathrm{Li}}}{N_{\mathrm{Li}}} \geq 15$, using $\frac{N_{0,\mathrm{Li}}}{N_{\mathrm{Li}}} \approx 1.5$ in equilibrium. We can therefore simplify the loading rate equation to:

$$\frac{dN_{\mathrm{Li}}}{dt} = L - \gamma_0 N_{\mathrm{Li}} - 2\beta' n_{0,\mathrm{Na}} N_{\mathrm{Li}}. \tag{4.2}$$

The solution to this equation, assuming $N_{\mathrm{Li}}(0) = 0$, is

$$N_{\mathrm{Li}}(t) = \frac{L}{\gamma_0 + 2\beta' n_{0,\mathrm{Na}}} (1 - e^{-(\gamma_0 + 2\beta' n_{0,\mathrm{Na}})\, t}).$$

Thus, from loading curves of the Li MOT with and without Na, we can extract β' in two ways: Measuring the number of atoms in both cases and measuring the loading time $\tau = \frac{1}{\gamma_0 + 2\beta' n_{0,\mathrm{Na}}}$ and $\tau_0 = \frac{1}{\gamma_0}$ with and without sodium:

$$\beta' = \frac{\gamma_0}{2 n_{0,\mathrm{Na}}} \left(\frac{N_{0,\mathrm{Li}}}{N_{\mathrm{Li}}} - 1 \right) \quad \text{and}$$

$$\beta' = \frac{1/\tau - 1/\tau_0}{2 n_{0,\mathrm{Na}}}.$$

From a fit to the data shown in fig. 4-7 using eq. 4.2, we have obtained an interaction cross-section of $\beta' = 10^{-12}\,\mathrm{cm}^3/\mathrm{s}$. This value, is in fair agreement with results on the cross-section between sodium and lithium-7 by Binder et. al. [41].

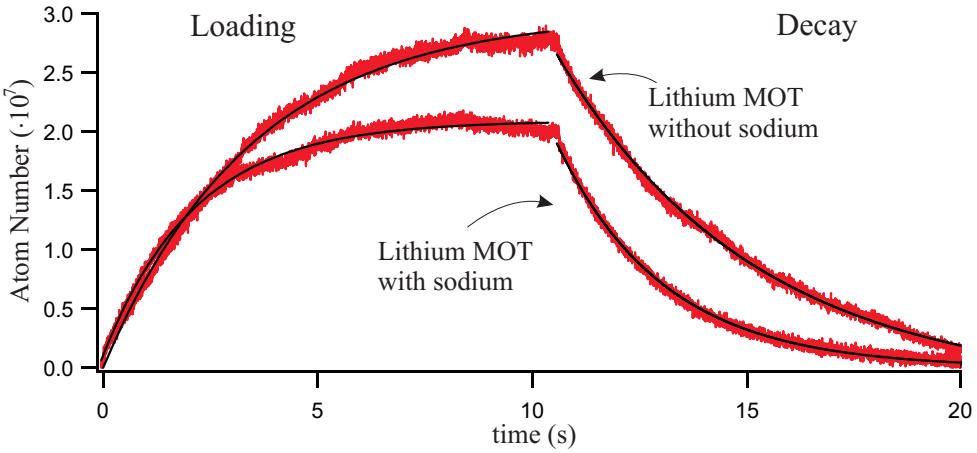

Figure 4-7: *Loading and Decay of the Li MOT with and without sodium being present. The data was obtained by imaging the fluorescence of the Li MOT onto a photodiode equipped with an interference filter for red light. A fit to the curves using eq. 4.2 gives a loading time of 3.5 s with and of 2.1 s without sodium, and peak values of 30 million atoms with and 20 million without sodium. Li atoms with and without Na.*

Chapter 5

Conclusion and Outlook

In this thesis I have described the building of a new double-species experiment involving ^{23}Na and ^{6}Li designed to cool fermionic lithium below the Fermi temperature.

To achieve the first cooling stage, slowing in a Zeeman slower and trapping in a magneto-optical trap, a diode laser system for ^{6}Li has been built. The frequencies created with the help of a grating stabilized master laser are amplified by four slave lasers of 30 mW output power, each being stabilized by injection locking. A frequency-stabilization scheme based on saturated absorption spectroscopy was implemented to reference the master laser to an atomic resonance. The stability of the master laser was estimated to be well below 1 MHz.

In order to image the atoms, resonant probe light was created by a Tandem-AOM technique which allows for a continuous frequency scan over resonance. This serves two similar goals: Firstly, an absorption monitor measures online the absorption of a weak laser beam going through the trapped cloud of atoms, while its frequency is swept over resonance in about 1 ms. This can be used to give an estimate of the number of atoms in the trap and also serves as a monitor when optimizing the MOT beam alignment. Secondly, resonant light is again sent through the cloud, either trapped in the MOT or in the magnetic trap. Its light is recorded on a CCD chip to take an absorption image of the atoms. This is how all the data on the atomic gas is taken.

With the help of absorption imaging, temperature measurements of the ^{6}Li-cloud in the MOT have been performed, giving a temperature of about 600 μK for a detuning of the MOT-frequency of $\delta = -22$ MHz. A first value for the cross-section of sodium and lithium in the double-species MOT has been estimated to be $10^{-12}\,\mathrm{cm}^3/\mathrm{s}$.

Prospects of Magnetic Trapping

From the measurements presented in the last chapter, we can see that the lithium cloud is too hot to be efficiently transferred to the magnetic trap in the $|F = 1/2, m_F = -1/2\rangle$. For that state, the trap-depth is limited to 300 μK due to the quadratic Zeeman shift (see section 2.5). Therefore, the plan is to trap lithium in the $|F = 3/2, m_F = 3/2\rangle$ stretched state with practically infinite trap-depth. Sodium, which is about 150 μK cold

after polarization gradient cooling, is supposed to sympathetically cool lithium. We hope that losses due to spin-exchange collisions are still moderate during that phase. The thus cooled sample of lithium atoms can then be transferred into the $|F = 1/2, m_F = -1/2\rangle$-state by a two-photon-transition, a microwave and a RF-pulse. In that state, further cooling with evaporatively cooled sodium can take place. So far we have achieved a transfer rate of 15% lithium-atoms in the $|F = 3/2, m_F = 3/2\rangle$-state.

Outlook

If evaporative cooling of sodium with lithium proves feasible, the next step would be to trap the ^{6}Li-atoms in an optical dipole trap with far red-detuned light. In such a trap, the light field induces a dipole moment in the atom which oscillates at the light frequency. This results in an ac-Stark shift of the atomic ground state, up for blue-detuned light, and down for light tuned to the red of resonance. With red-detuned light, one thus creates a potential minimum for the atoms at maxima of the light intensity.
A dipole trap provides long confinement times in a conservative potential and ideal conditions for measurements on elastic collisions. We could trap two states of ^{6}Li with different magnetic moment. Magnetic fields, no longer needed for trapping, can be used to change the cross section for collisions between the two states. It is expected to find a so-called Feshbach resonance for the cross section at about 800 G [40]. This will be useful in the search for the BCS phase transition, since a larger scattering length will increase the transition temperature for Cooper pairing (eq. 1.1).

Appendix A

Laser System

Appendix B

Locking signal

To calculate the lineshape generated by the lock-in-amplifier one has to evaluate the Fourier transform of the modulated saturated absorption signal. The lamb-dips and the cross-over are Lorentzian and of the form $f(\omega) \propto \frac{1}{1+4(\frac{\omega-\omega_0}{\Gamma})^2}$, with Γ the linewidth of the signal and ω_0 the center frequency. To simplify the following formulas, we count ω in multiples of $\Gamma/2$ relative to the center frequency. Let the modulating frequency be $\omega_{\rm LO}$, the amplitude of the modulation $\Delta\omega$. We have to evaluate the integral:

$$I(\omega, \Delta\omega) = \frac{2}{T}\int_0^T dt\, \cos(\omega_{\rm LO} t)\, f(\omega + \Delta\omega\cos(\omega_{\rm LO} t)).$$

For $T \gg 1/\omega_{\rm LO}$ we can integrate over one period:

$$\begin{aligned} I(\,\omega, \Delta\omega) &= \frac{1}{\pi}\int_0^{2\pi} d\phi\, \cos\phi\, f(\omega + \Delta\omega\cos\phi) \\ &= \frac{1}{\pi}\int_0^{2\pi} d\phi\, \frac{\cos\phi}{1 + (\omega + \Delta\omega\cos\phi)^2} \\ &= \Re\frac{1}{2\pi}\int_0^{2\pi} d\phi\, \left(\frac{e^{\mathrm{i}\phi}}{1 + \mathrm{i}(\,\omega + \Delta\omega\cos\phi)} + \frac{e^{\mathrm{i}\phi}}{1 - \mathrm{i}(\,\omega + \Delta\omega\cos\phi)}\right). \end{aligned}$$

In the following we integrate the first of the above terms, the second is obtained from that result by changing $\omega \to -\omega$, $\Delta\omega \to -\Delta\omega$. We now express $\cos\phi$ in terms of $z \equiv e^{\mathrm{i}\phi}$ and change the variable of integration to z:

$$\begin{aligned} I(\omega, \Delta\omega) &= \Re\frac{1}{2\pi}\int_0^{2\pi} d\phi\, \frac{e^{\mathrm{i}\phi}}{1 + \mathrm{i}(\omega + \frac{\Delta\omega}{2}(e^{\mathrm{i}\phi} + e^{-\mathrm{i}\phi}))} + (\omega, \Delta\omega \to -\omega, -\Delta\omega), \\ &= \Re\frac{1}{2\pi\mathrm{i}}\oint_{|z|=1} dz \frac{1}{1 + \mathrm{i}(\omega + \frac{\Delta\omega}{2}(z + z^{-1}))} + (\omega, \Delta\omega \to -\omega, -\Delta\omega), \\ &= \Re\frac{1}{2\pi\mathrm{i}(1+\mathrm{i}\omega)}\oint_{|z|=1} dz\, \frac{z}{z + \frac{\mathrm{i}\Delta\omega}{2(1+\mathrm{i}\omega)}(1 + z^2)} + (\omega, \Delta\omega \to -\omega, -\Delta\omega). \end{aligned}$$

z goes around the unit circle when ϕ changes from 0 to 2π. Following Cauchy's residue theorem the value of the integral is determined by the poles of the integrand lying in the unit circle. If we denote $a = \frac{\mathrm{i}\Delta\omega}{1+\mathrm{i}\omega}$, the poles of the integrand are:

$$z_{1,2} = -\frac{1}{a} \pm \sqrt{\frac{1}{a^2} - 1}$$

Without proof we state that for $\omega > 0$ it is the first pole which lies in the unit circle, for $\omega < 0$ it is the second. We obtain:

$$\begin{aligned} I(\omega, \Delta\omega) &= \Re \frac{1}{1+\mathrm{i}\omega} \mathrm{Res}_{z_{1,2}} \frac{z}{z + \frac{a}{2}(z^2+1)} + (\omega, \Delta\omega \to -\omega, -\Delta\omega) \\ &= \Re \frac{1}{\mathrm{i}\Delta\omega} (1 \mp \frac{1}{\sqrt{1-a^2}}) + (\omega, \Delta\omega \to -\omega, -\Delta\omega) \end{aligned}$$

The first term of this expression is canceled by the corresponding term with $\Delta\omega \to -\Delta\omega$. The square root in the second term can be written as

$$\begin{aligned} \sqrt{1-a^2} &= \sqrt{1 + \frac{\Delta\omega^2}{(1+\mathrm{i}\omega)^2}} = \sqrt{1 + q(1-\mathrm{i}\omega)^2} \quad \text{with} \quad q = \frac{\Delta\omega^2}{(1+\omega^2)^2} \\ &= \sqrt{|1 + q(1-\mathrm{i}\omega)^2|} \cdot e^{\mathrm{i}\frac{\phi}{2}} \quad \text{where} \quad \cos\phi = \frac{1 + q(1-\omega^2)}{|1 + q(1-\mathrm{i}\omega)^2|} \end{aligned}$$

and therefore

$$\begin{aligned} I(\omega, \Delta\omega) &= \mp \frac{1}{\mathrm{i}\Delta\omega} \frac{e^{-\mathrm{i}\frac{\phi}{2}} - e^{\mathrm{i}\frac{\phi}{2}}}{\sqrt{|1 + q(1-\mathrm{i}\omega)^2|}} \\ &= \mp \frac{2}{\Delta\omega} \frac{-\sin\frac{\phi}{2}}{((1 + q(1-\omega^2))^2 + 4q^2\omega^2)^{\frac{1}{4}}} \end{aligned}$$

Since $\sin^2\frac{\phi}{2} = \frac{1-\cos\phi}{2}$ this becomes finally:

$$I(\omega, \Delta\omega) = -\frac{\omega}{|\omega|} \frac{\sqrt{2}}{\Delta\omega} \frac{\sqrt{\sqrt{(1 + q(1-\omega^2))^2 + 4q^2\omega^2} - (1 + q(1-\omega^2))}}{\sqrt{(1 + q(1-\omega^2))^2 + 4q^2\omega^2}}. \tag{B.1}$$

One can verify that for small modulating amplitudes, eq. B.1 reduces to the same result as discussed in the text:

$$I(\omega, \Delta\omega) \simeq -2\omega \frac{\Delta\omega}{(1+\omega^2)^2} = \Delta\omega \cdot f'(\omega).$$

The resulting signal is proportional to the derivative of the line shape.

Appendix C

PI-Controller

PI-Controller for Frequency Stabilization

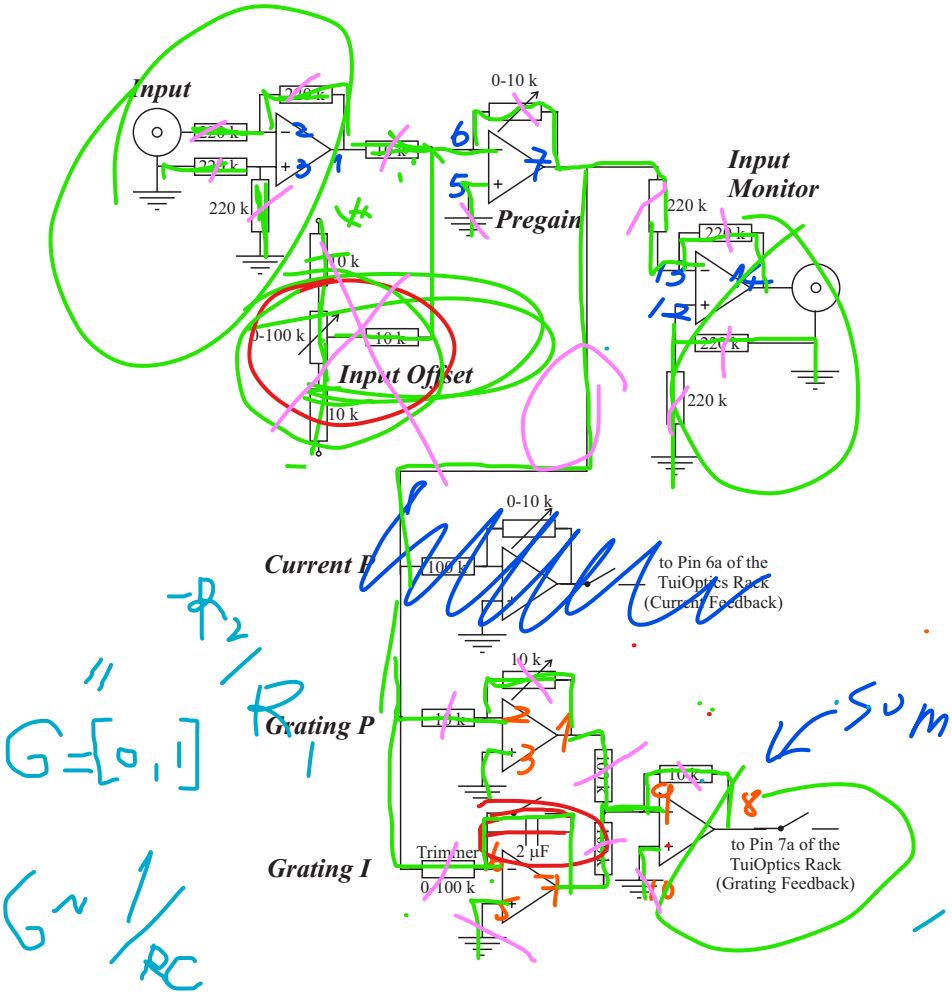

Figure C-1: *Electronic circuit of the PI-Controller for the frequency stabilization. It features an input monitor, a pregain stage, proportional and integral (time constant 2.5 s) feedback for the PZT which adjusts the length of the lasers external cavity, as well as proportional gain for current feedback.*

PI-Controller for Intensity Stabilization

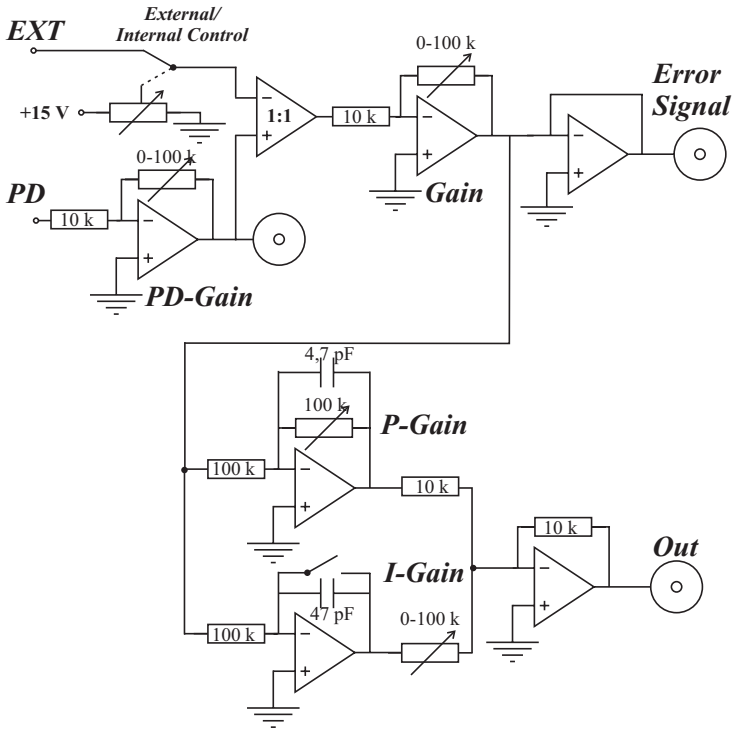

Figure C-2: *Electronic circuit of the PI-Controller for the Intensity Stabilization. It features an photodiode monitor, a gain stage for the error signal, an error monitor and proportional and integral (time constant 30 μs) feedback.*

Bibliography

[1] M.H. Anderson *et al.*, Science **269**, 198(1995); K.B. Davis *et al.*, *Phys. Rev. Lett.* **75**, 3969 (1995); C.C. Bradley *et al.*, *Phys. Rev. Lett.* **75**, 1687 (1995); C. C. Bradley *et al.*, *Phys. Rev. Lett.* **78** 985 (1997); D. G. Fried *et al.*, *Phys. Rev. Lett.* **81**, 3811 (1998); A. Robert *et al.*, *Science* 292, 461 (2001); F. Pereira Dos Santos *et al.*, *Phys. Rev. Lett.* **86**, 3459 (2001);

[2] B. DeMarco and D.S. Jin. Onset of Fermi Degeneracy in a Trapped Atomic Gas. *Science*, 285:1703,1999

[3] S. Inouye, M.R. Andrews, J. Stenger, H.-J. Miesner, D.M. Stamper-Kurn and W. Ketterle. Observation of Feshbach resonances in a Bose-Einstein condensate. *Nature*, 392(0):151, March 1998

[4] W. Ketterle, D.S. Durfee and D.M. Stamper-Kurn, in Proceedings of the International School of Physics "Enrico Fermi", *Bose Einstein condensation in Atomic Gases*, M. Inguscio, S. Stringari, and C. Wieman Eds. (IOS Press, Amsterdam 1999)

[5] B. DeMarco and D.S. Jin, *Phys. Rev. A* **58**, R4267 (1998)

[6] B. DeMarco *et al.*, *Phys. Rev. Lett.* **82**, 4208 (1999)

[7] B. DeMarco, S.B. Papp, and D.S. Jin. Pauli Blocking of Collisions in a Quantum Degenerate Atomic Fermi Gas. *Phys. Rev. Lett.* **86**, 24, 5409 (2001)

[8] Andrew G. Truscott et al., Science Express 1 March 2001, 10.1126/science.1059318

[9] F. Schreck, G. Ferrari, K.L. Corwin, J. Cubizolles, L. Khaykovich, M.-O. Mewes, and C. Salomon. Sympathetic Cooling of Bosonic and Fermionic Lithium Gases towards Quantum Degeneracy. *Phys. Rev. A* **6**4, 011402(R) (2001)

[10] C. Raman, M. Köhl, R. Onofrio, D.S. Durfee, C.E. Kuklewicz, Z. Hadzibabic and W. Ketterle. Evidence for a Critical Velocity in a Bose-Einstein Condensed Gas. *Phys. Rev. Lett.*, 83(13):2502 (1999)

[11] K.W. Madison, F. Chevy, W. Wohlleben, J. Dalibard. Vortex formation in a stirred Bose-Einstein condensate. *Phys. Rev. Lett.* **84**, 806 (2000)

[12] J.R. Abo-Shaeer, C. Raman, J.M. Vogels, and W. Ketterle. Observation of Vortex Lattices in Bose-Einstein Condensates. *Science* 292, 476-479 (2001)

[13] E.R.I. Abraham, W.I. McAlexander, J.M. Gerton, R.G. Hulet, R. Côté and A. Dalgarno. Triplet s-wave resonance in ^{6}Li collisions and scattering lengths of ^{6}Li and ^{7}Li. *Phys. Rev. A*, 55(5):R3299, Mai 1997

[14] G. Breit and I.I. Rabi. Measurement of nuclear spin. *Physical Review*, 38:2082, 1931

[15] S. Chu, L. Hollberg, J. Bjorkholm, A. Cable, and A. Ashkin. Three-Dimensional Viscous Confinement and Cooling of Atoms by Resonance Radiation Pressure. *Phys. Rev. Lett.* **5**5, 48 (1985)

[16] D.J. Wineland, W.M. Itano. Laser Cooling of Atoms. *Phys. Rev. A* **20**:4, 1521 (1979)

[17] P.D. Lett, R.N. Watts, C.I. Westbrook, and W.D. Phillips. Observation of Atoms Laser Cooled below the Doppler Limit. *Phys. Rev. Lett.* **61**, 169 (1988)

[18] J. Dalibard et C. Cohen-Tannoudji. Laser Cooling Below the Doppler Limit by Polarization Gradients – Simple Theoretical Models. *J. Opt. Soc. Am. B* **6**, 2023-2045 (1989)

[19] P.J. Ungar, D.S. Weiss, E. Riis, S. Chu. Optical molasses and ultilevel atoms: theory. J. Opt. Soc. Am. B **6**, 2058-71 (1989)

[20] See note at the end of [21]

[21] E.L. Raab, M. Prentiss, A. Cable, S. Chu, and D.E. Pritchard. Trapping of Neutral Sodium Atoms with Radiation Pressure. *Phys. Rev. Lett.* **59**, 23, 2631-2634 (1987)

[22] W. Phillips and H. Metcalf. Laser Deceleration of an Atomic Beam. *Phys. Rev. Lett.* **48**, 596 (1982).

[23] H.J. Metcalf et P. van der Straten. Laser Cooling and Trapping. *Springer, New York*

[24] W.H. Wing. On neutral particle trapping in quasistatic electromagnetic fields. *Prog. Quant. Electr.* **8**, 181 (1984)

[25] Y.V. Gott, M.S. Ioffe, and V.G. Tel'kovskii. *Nuclear Fusion Supplement* **3**, 1045 (1962)

[26] D.E. Pritchard. Cooling Neutral Atoms in a Magnetic Trap for Precision Spectroscopy. *Phys. Rev. Lett.* **51**, 1336 (1983)

[27] H.F. Hess, G.P. Kochansky, J.M. Doyle, N. Masuhara, D. Kleppner, and T.J. Greytak. Magnetic Trapping of Spin-Polarized Atomic Hydrogen. *Phys. Rev. Lett.* **59**(6):672, 1987

[28] S. Chu. Manipulating of neutral particles. *Rev. Mod. Phys.* **70**, 3, 685-706 (1998)

[29] W.D. Phillips. Laser Cooling and trapping of neutral atoms. *Rev. Mod. Phys.* **70**, 3, 721-741 (1998)

[30] C. Cohen-Tannoudji. Manipulating Atoms with Photons. *Rev. Mod. Phys.* **70**, 3, 707-719 (1998)

[31] W. Ketterle and N.J. van Druten. Evaporative cooling of trapped atoms. *Advances in Atomic, Molecular, and Optical Physics*, 37:181, 1996

[32] C.H. Henry. Theory of the linewidth of semiconductor lasers. *IEEE Journal of Quantum Electronics*, QE-18(2):259-264, 1982

[33] J.P. Bouyer. Spectral stabilization of an InGaAsP laser by injection-locking. *Annales de Physique*, 18(2):89-240, April 1993

[34] A.E. Siegman. Lasers. University Science Books, Mill Valley, CA, USA, 1986

[35] C.E. Wieman, L. Hollberg, Rev. Sci. Intstr. 62 (1991) 1.

[36] L. Ricci, M. Weidemüller, T. Esslinger, A. Hemmerich, C. Zimmermann, V. Vuletic, W. König, T.W. Hänsch, Optics Comm. 117 (1995) 541

[37] C.G. Townsend, N.H. Edwards, C.J. Cooper, K.P. Zetie, C.J. Foot, A.M. Steane, P. Szriftgiser, H. Perrin, J. Dalibard, Phys. Rev. A 52 (1995) 1423

[38] W. Ketterle, D.S. Durfee, and D.M. Stamper-Kurn. Making, Probing and understanding Bose-Einstein condensates. In M. Inguscio, S. Stringari and C.E. Wieman eds., *Bose-Einstein Condensation in Atomic Gases*, Proceedings of the "Enrico Fermi" Summer School, July 1998, Varenna, Italy.

[39] U. Schünemann, H. Engler, M. Zielonkowski, M. Weidemüller, R. Grimm. Magneto-optic trapping of lithium using semiconductor lasers. Optics Comm. 158 (1998) 263

[40] M. Houbiers, H.T.C. Stoof, W.I.McAlexander and R.G. Hulet. Elastic and inelastic collisions of Li-6 atoms in magnetic and optical traps. *Phys. Rev. A*, 57(3):R1497, March 1998

[41] C. Binder, V. Wippel, L. Windholz. Interaction between Na and Li atoms in a two-species MOT. *Workshop Quantum Gases 2001*, to be published

[42] J. Weiner, V.S. Bagnato, S.C. Zilio, and P.S. Julienne. *Rev. Mod. Phys.* **7**1, 1 (1999)

[43] G.D. Telles, W. Garcia, L.G. Marcassa, and V.S. Bagnato, D. Ciampini, M. Fazzi, J.H. Müller, D. Wilkowski, and E. Arimondo. Trap loss in a two-species Rb-Cs magneto-optical trap. *Physical Review A* **6**3, 033406-1 (2001)

Summary

This thesis deals with the cooling and trapping of a mixture of two different atomic species, sodium and fermionic lithium. For this goal, an existing experiment for Bose-Einstein-condensation of sodium has been extended by a two-species oven and a laser system for laser cooling of lithium. The subject of this thesis is the development and building of this laser system, as well as first measurements of the number and temperature of the lithium atoms in the magneto-optical trap. A first estimate on the cross-section between Na and ^{6}Li in the MOT is presented.

The quantum nature of indistinguishable particles gets important, when at extremely low temperatures and high densities the thermal wavelength becomes comparable to the average distance between two particles. Bosons, particles with integer spin, hereby undergo a phase transition, the so-called Bose-Einstein-Condensation. Here, a macroscopic fraction of particles occupies the ground state of the system. For Fermions, particles with half-integer spin, it is impossible to occupy the same quantum mechanical state due to the Pauli-exclusion principle. They are forced to distribute themselves over different states.
This quantum degenerate behaviour was, until several years ago, only known to occur in strongly interacting systems, which made the theoretical description of the underlying physics extremely difficult. It is therefore interesting to create quantum degenerate systems with only weak interactions between the particles. With the help of technologies for the creation of ultra-cold atoms, developed only in the last two decades, in 1995 Bose-Einstein-Condensation in a dilute, weakly interacting atomic gas was achieved [1].
The natural extension of these methods to a gas of Fermions encounters difficulties. The last step to reach the critical temperature, evaporative cooling, is prohibited by Fermi statistics, since needed elastic collisions between the atoms are strongly suppressed. Experiments in quantum degeneracy of Fermions therefore tend to use two different atomic species, for example the two natural isotopes of lithium [8, 9]. The Bosons are cooled evaporatively, whereas the Fermions are brought to thermal equilibrium trough collisions with their bosonic partners. The experiment described in this thesis uses sodium and fermionic lithium to reach the quantum degenerate regime.

The thesis is divided in the following parts: After the introduction, chapter two outlines the theoretical basics of the different experimental methods to cool and trap the atoms. Chapter three describes the building of the needed laser system for lithium, where the main part is dedicated to the frequency stabilization and the creation of the imaging light. In chapter four we summarize first measurements on the atom number and temperature of the lithium atoms in the magneto-optical trap (MOT), and present a first

estimate on the cross-section between Lithium and Sodium in the MOT. The conclusion found in chapter five gives an outlook to future experiments.

Resumé

Le sujet de cette thèse est le refroidissement et le piégeage d'un mélange de deux espèces atomiques, le sodium et le lithium fermionique. Pour ce but, une expérience existante a été étendu par un four à double-espèce et un système laser pour le refroidissement laser du lithium. Cette thèse décrit le développement et le montage de ce système laser, ainsi que des premières mesures de la température des atomes de lithium dans le piège magnéto-optique (PMO). Une première estimation de la section efficace entre lithium et sodium dans le PMO est présentée.

La nature quantique des particules indiscernables devient importante à basse température, si la densité est assez grande: la longueur d'onde thermique devient comparable à la distance moyenne entre les particules. Pour les Bosons, particules avec un spin entier, il se produit une transition de phase, la condensation de Bose-Einstein. Une fraction importante des atomes s'accumule dans létat fondamental du système. Au contraire, le principe d'exclusion de Pauli interdit à deux fermions identiques d'occuper le même état. Ils sont forcé à se répartir sur des états quantiques différents.
Ce comportement de dégénération quantique était observé jusqu'il y a quelques années uniquement dans des systèmes aux fortes interactions, ce qui a rendu les déscriptions théoriques de tels systèmes très difficiles. Pour cela il est intéressant de créer des systèmes à dégénération quantique où les interactions entre les particules restent faibles. A l'aide des techniques pour la création des atomes ultra-froids, développés dans les deux dernières décades, on a réussi pour la première fois en 1995 de créer un condensat de Bose-Einstein dans un gaz atomique dilué dans un piège magnétique [1].
L'ètendance naturelle de ces méthodes sur un gaz de Fermions rencontre des difficultés. La dernière étappe pour arriver à la température critique, le refroidissement "evaporatif", est interdit par la statistique de Fermi. Les collisions élastiques entre les atomes sont largement supprimé. Pour cela, les expériences sur la dégénération quantique des Fermions dans des gaz atomiques ultra-froids utilisent frequemment deux espèce atomiques, par exemple les deux isotopes naturelles de lithium [8, 9]. Les Bosons sont refroidit "évaporativement", les fermions thermalisent avec les partenaires bosoniques par collisions. L'expérience présenté dans cette thèse utilise le sodium et le lithium-6 fermionique pour pénetrer dans le régime de dégénération quantique.

Cette thèse est repartie dans les parties suivantes: Après l'introduction, le chapitre deux présente les élements de base théorique des méthodes expérimentals du refroidissement et du piégeage des atomes. Le chapitre trois décrit le montage du systéme laser pour le lithium. La plus grande partie est consacrée à la stabilisation de fréquence des lasers et

au système d'imagérie. Les premières mesures du nombre atomique et de la température des atomes dans le piège magnéto-optique (PMO) sont présenté dans le chapitre quatre, ainsi quune première estimation de la section efficace entre le lithium et le sodium dans le PMO. La conclusion en chapitre cinque donne une perspective aux expériences futurs.

Zusammenfassung

Diese Arbeit behandelt das Kühlen und den Einfang eines Gemischs zweier verschiedener atomarer Spezies, Natrium und fermionisches Lithium. Dazu wurde ein bestehendes Experiment zur Bose-Einstein-Kondensation von Natrium durch einen Zwei-Spezies-Ofen und ein Lasersystem zur Laserkühlung von Lithium erweitert. Die Entwicklung und der Aufbau dieses Lasersystems, erste Temperaturmessungen der Lithium-Atome in der magneto-optischen Falle (MOT) sowie eine erste Abschätzung des Wirkungsquerschnitts zwischen Natrium und Lithium in der MOT sind der Inhalt dieser Arbeit.

Die Quantennatur ununterscheidbarer Teilchen tritt dann zu Tage, wenn bei extrem tiefen Temperaturen und hoher Dichte die thermische Wellenlänge vergleichbar groß wird wie der mittlere Abstand zwischen zwei Teilchen. Für Bosonen, Teilchen mit ganzzahligem Spin, findet hierbei ein Phasenübergang statt, die sog. Bose-Einstein-Kondensation. Hierbei nimmt eine makroskopische Anzahl von Teilchen den Grundzustand des Systems ein. Nach dem Pauli-Verbot ist es im Gegensatz dazu für zwei identsiche Fermionen, Teilchen mit halbzahligem Spin, unmöglich, ein und den selben Zustand einzunehmen. Sie sind gezwungen, sich auf verschiedene quantenmechanische Zustände zu verteilen.
Dieses quantenentartete Verhalten zeigte sich bis vor wenigen Jahren nur in stark wechselwirkenden Systemen, was ihre theoretische Beschreibung extrem erschwert. Interessant ist es daher, quantenentartete Systeme mit möglichst kleinen Wechselwirkungen zu erzeugen. Mit Hilfe der erst in den letzten beiden Jahrzehnten entwickelten Technologien zur Erzeugung ultrakalter Atome gelang es 1995 zum ersten Mal, eine Wolke schwach wechselwirkender, magnetisch gefangener Atome in ein Bose-Einstein-Kondensat zu überführen [1].
Die natürliche Erweiterung dieser Methoden auf ein Gas von Fermionen gelingt nicht problemlos. Der letzte Schritt zum Erreichen der kritischen Temperatur, das Verdampfungs- oder evaporatives Kühlen, wird durch die Fermistatistik verhindert, da die erforderlichen elastischen Stöße zwischen den Atomen weitgehend ausbleiben. Experimente zur Quantenentartung von Fermionen in ultrakalten Gasen verwenden daher zunehmend zwei verschiedene atomare Spezies, z.B. die beiden in der Natur vorkommenden Isotope des Lithium [8, 9]. Die Bosonen werden evaporativ gekühlt, während die Fermionen durch Stöße mit den bosonischen Partnern mit diesen ins thermische Gleichgewicht gebracht werden. Das in dieser Arbeit vorgestellte Experiment verwendet Natrium und fermionisches Lithium-6, um in das quantenentartete Regime vorzudringen.

Die Arbeit ist in folgende Abschnitte unterteilt: Nach der Einleitung faßt Kapitel zwei kurz die theoretischen Grundlagen der verschiedenen experimentellen Methoden zur Kühlung und dem Einfang von Atomen zusammen. Kapitel drei beschreibt den Aufbau

des benötigten Lasersystems für Lithium, wobei der Schwerpunkt auf die Frequenzstabilisierung der Laser und das Abbildungssystem gelegt wurde. In Kapitel vier werden Messungen zur Atomzahl und zur Temperatur der Lithium-Atome in der magneto-optischen Falle (MOT) zusammengetragen, und eine erste Abschätzung des Wirkungsquerschnitts zwischen Lithium und Natrium in der MOT gegeben. Im fünften Kapitel wird die Arbeit zusammengefaßt und ein Ausblick auf nachfolgende Experimente gegeben.

Acknowledgements

My time at MIT was an enormously exciting experience, both scientifically - that might be obvious - and on the personal side - which is not so obvious. I had the privilege and pleasure to work with an extraordinary group of people in a young and fascinating field of physics.

My deepest gratitude goes to Wolfgang Ketterle, who gave me this unique opportunity. Through his steady encouragement and support, I discovered the joy of experimental physics, the world of ultra-cold bosons and fermions, and a new insight to science in general. I am grateful for the conferences I was able to attend (including a terrific soccer match) and for his efforts related to this thesis (e.g. teaching me how to align an AOM in no time to 90% efficiency).

I was incredibly fortunate to team up with Zoran Hadzibabic, Claudiu Stan, Deep Gupta and Kai Dieckmann. Most of my days and sleepless nights I spent with Zoran building the laser system, literally twice, but also colonizing unknown worlds on distant shores. From the first day, he treated me as a graduate student and equal partner, and partnership transformed into close friendship. He combines brilliant and original thoughts with a good taste when it comes to the decision on what to have for dinner. His positive influence on my thinking about both physics and general life issues cannot be overestimated. I would have liked to compromise the diet lasers a little bit further, but, who knows, there are always many escape channels.

No part of this work would have been possible without the original, aesthetic work of Claudiu. We simply would not have any atoms. He designed and built the lithium vapor cell, at the heart of the laser stabilization. His excellence when dealing with ultra high vacuum technology was already proven by the atomic beam line and Zeeman slower he built for the first lithium-only experiment. The finishing of the double-species oven triggered our move to the "old" BEC machine, and the curvature of our "efficiency"-curve increased significantly. I also like to thank him for the most beautiful day in these months, our great trip to Martha's Vineyard, as well as for the critical reading of the manuscript.

When we merged the red with the yellow photons, we could fully rely on Deep's expertise with the BEC machine and the dye laser system. I thank him for the infinite amount of time he spent on literally squeezing the maximum of power out of the dye. With him, Zoran and I have also found another companion for early breakfasts at Fresco's.

Soon after my arrival, Kai joined the group as a new postdoc. He brought all his experience on BEC and his knowledge on laser diodes from Amsterdam. Besides, he is the only one in the lithium group who shares my addiction to coffee, even bad one. I am

grateful for his help with the electronics and for his support during writing of this thesis.

Thanks also go to Axel Görlitz, who supervised the lithium work before his leave.

One big advantage of working in this group is the critical mass of knowledgeable people. To almost any question ranging from electronic circuits to atom interferometry one can find one member next door who knows the answer. Therefore, I would like to thank Jamil Abo-Shaeer, with whom I also share a bright memory on canadian nights at the Ceep's, Aaron Leanhardt, who introduced me to baseball and beat me too often in pool, Chandra Raman, who inspired the chosen intensity stabilization circuit, Todd Gustavson, who helped with the PI-Controller, as well as Micah Boyd, Ananth Chikkatur, Shin Inouye, Till Rosenband, Erik Streed, Dominik Schneble, Yoshio Torii, Johnny Vogels and Kaiwen Xu.

I also want to express my thanks to Carol Costa, for all the help with the bureaucracy and those relaxing chats from time to time.

I should also thank the tireless effort of several delivery services, most notably Dimitrio's Cuisine, 272 Brookline Street, directly followed by Cinderella's, 901 Main Street, both Cambridge, Laverde's for the coffee supplies, and Fresco's for relaxing breakfasts.

I owe the greatest debt to my family who encouraged me throughout my studies and adopted my many problems as their own. Their support has always given me strength and confidence.

For the organization of the "stage long" I express my thanks to Jean-Michel Raimond, Laurence Rezeau and Pierre-François Cohadon. I would also like to thank the French state for the possibilities given to European students through its financial support of the Normaliens.

In addition I would like to acknowledge the Studienstiftung des deutschen Volkes for their support.